NASA CONTRACTOR REPORT

NASA CR-113

NASA CR-1132

DRAG ASSOCIATED WITH SEPARATED FLOW OVER TWO-DIMENSIONAL V-SHAPED NOTCHES UNDER TRANSONIC AND SUPERSONIC CONDITIONS

by Ronald H. Howell and Helmut H. Korst

Prepared by
UNIVERSITY OF ILLINOIS
Urbana, Ill.
for

NATIONAL AERONAUTICS AND SPACE ADMINISTRATION • WASHINGTON, D. C. • SEPTEMBER 1968

DRAG ASSOCIATED WITH SEPARATED FLOW OVER TWO-DIMENSIONAL V-SHAPED NOTCHES UNDER TRANSONIC AND SUPERSONIC CONDITIONS

By Ronald H. Howell and Helmut H. Korst

Prepared under Grant No. NSG-13 by
~~UNIVERSITY OF~~ ILLINOIS Univ.
Urbana, Ill.

for

NATIONAL AERONAUTICS AND SPACE ADMINISTRATION

For sale by the Clearinghouse for Federal Scientific and Technical Information
Springfield, Virginia 22151 – CFSTI price $3.00

SUMMARY

The major objectives of this investigation were to seek an understanding of the flow mechanisms and the controlling parameters for flow in v-shaped notches and the development of experimental methods for measuring the drag of v-shaped notches. The wall geometry was limited to two-dimensional symmetric notches defined by specifying the length and angle of the notch. For any given notch geometry the free stream Mach number was the primary variable while the viscous effects, specified by the boundary layer momentum thickness and the length Reynolds number, were secondary variables. The Mach number range investigated was from 0.5 to 1.2 and at 2 while the approaching boundary layer was always turbulent and reasonably well representative of fully developed shear layers along adiabatic flat plates with the momentum thickness Reynolds number in the range from 7500 to 15000.

In order to cover a wide range of boundary layer momentum thickness to notch depth ratios, experiments were carried out with notches of various lengths (3.5 in., 2.25 in., 1 in., 0.675 in., and 0.375 in.) and notch angles (7°, 10°, 13°, and 16°).

Schlieren observations, pressure distributions, and direct drag force measurements (with a specially developed drag force balance) contributed to a better understanding of the viscid-inviscid flow phenomena controlling the drag of notches and the redevelopment of the boundary layer downstream of the disturbance.

TABLE OF CONTENTS

SYMBOLS

a	velocity of sound
A	area
$\overline{A}$	total clearance area around perimeter of model
b	width of plate
C	Crocco number, velocity/maximum velocity
C_d	drag force/$\frac{1}{2}\rho_e u_e^2 bL$
C_f	wall shear stress/$\frac{1}{2}u_e^2\rho_e$
C_F	drag force/$\frac{1}{2}\rho_e u_e^2 A$
C_{wave}	partial drag component in supersonic flow
C_{trav}	partial drag component in subsonic and supersonic flow
d	vertical distance to separation point
$\overline{d}$	flat plate clearance between plate and base
D	drag force
D_{fp}	drag force on flat surface equal to the redevelopment length at same tunnel location, but without the notch upstream
F	drag force on plate of finite length
G	leakage flow rate
h	notch depth
H	boundary layer shape parameter, δ^*/θ
I_{2_j}	integral of a function of ϕ with respect to η
J	shear stress function
$\mathcal{J}$	transonic similarity parameter
k	transonic similarity parameter
k	ratio of specific heats

$\overline{K}$	calibration constant
L	plate length or notch length
M	Mach number
p	pressure
P	pressure
r	depth of the notch or cavity
R	specific gas constant
Re_θ	momentum thickness Reynolds number
Re_x	length Reynolds number
$\overline{t}$	time
T	temperature
U	free stream velocity in x-direction
u	velocity component in x-direction
$\overline{V}$	volume
v	velocity component in y-direction
x	coordinate along the plate or notch surface
y	coordinate normal to the plate or notch surface
δ	boundary layer thickness
δ^*	boundary layer displacement thickness
δ_2	boundary layer thickness at separation
η_p	position parameter
Ω	notch angle
ψ	dimensionless x-distance
ν	kinematic viscosity
μ	dynamic viscosity

ϕ	velocity ratio, u/u_e
ρ	density
τ	shear stress
θ	boundary layer momentum thickness
$\Delta\theta$	difference in boundary layer momentum thickness

Subscripts

e	free stream condition
1	first point along a flat plate
2	second point along a flat plate
o	stagnation conditions
i	incompressible fluid
d	downstream
u	upstream
n	notch
j	dividing streamline

1. INTRODUCTION

As the speed of aircraft increases toward sonic velocity and further into the supersonic regime accurate information about local details in the surface configuration of the aircraft assume great importance. A better understanding of lift and drag force contributions by disturbances as well as knowledge of the detailed flow mechanisms which determine aerodynamic stress distributions and heat transfer characteristics near such disturbances is necessary. Not only the exact geometry of the walls but the details of the approaching and adjacent flow fields assume a major role in determining the solution to the problem.

In contrast to rather well defined boundary conditions (walls) for attached flows the occurrence of separation often allows major adjustments in the flow geometry as a consequence of small changes in flow conditions. Where flow separation is a prominent feature and where the dynamics of the flow field are the results of interactions between hydrostatic and viscous stresses associated with attached and free shear layers, understanding has remained incomplete in spite of proposed flow models and their utilization in analytical approaches. Examples of such theoretical models include those proposed by Crocco and Lees (Reference 13), Lees and Reeves (Reference 34), Chapman (Reference 8) and Korst (Reference 29).

Subject of the study is the increase in the drag force due to the presence of a v-shaped notch in a flat surface. Diagram 1 defines the wall gemoetry together with the free stream and approaching flow conditions in the boundary layer. The wall geometry was

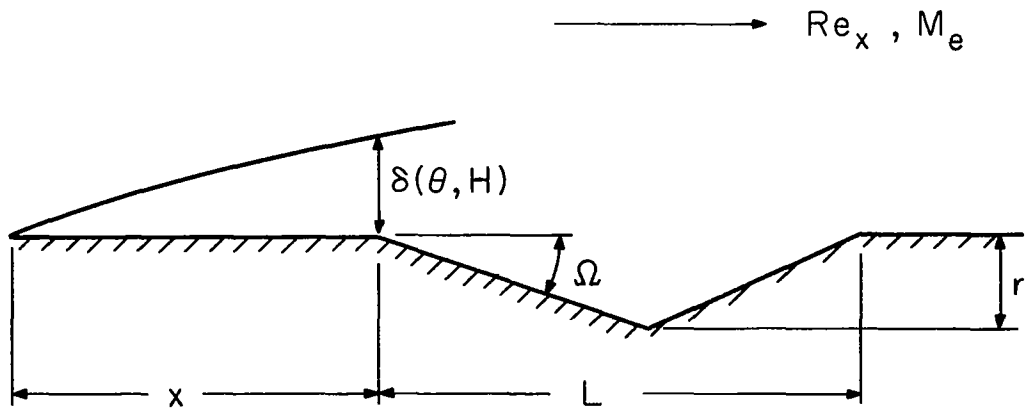

Diagram 1. Notch Geometry and Flow Variables

two dimensional and remained restricted to symmetrical notches; the approaching boundary layer was always turbulent and free stream conditions could be varied over a wide range in the transonic regime with additional experiments conducted at Mach numbers near two.

As indicated above the major objective in this investigation was the determination of the drag of a v-shaped notch; however, it was attempted to distinguish between the individual contributions of form drag and friction drag. This was particularly important for explaining the displacement and reduction from theoretical peak values of the drag coefficient near Mach number of unity. In addition, the shear drag of the redeveloping boundary layer downstream of the notch was evaluated.

Resonant conditions which are often observed for flows past relatively deep cavities (Ref. 43) were not evident during this investigation of rather shallow v-notches.

2. FLOW CONFIGURATION

A flow model has been devised which is made up of several different flow components. The concept of the model was derived from experimental observations of the flow over v-shaped notches, and the components were so chosen that simple interactions between them could be treated.

2.1 Qualitative Observations

While the flow configuration depicted in Fig. 1 was typical in a qualitative sense for a wide range of notch geometries and flow conditions, certain systematic changes can be pointed out which result from changes in the notch geometry and external flow conditions. The four basic variables in this problem are free stream Mach number, notch angle, Reynolds number, and the ratio of the approach boundary layer momentum thickness to the notch length.

Schlieren photographs of flow over a v-notch for constant approaching external free stream Mach numbers are shown in Figs. 2 and 4. Fig. 2 contains a series of photographs of flow at a Mach number of two over a two-inch long v-shaped notch with different notch angles. Fig. 4 contains schlieren photographs of flow at a Mach number of 1.14 over two-inch long notches with each photograph showing a different angle v-notch. As the notch angle Ω was increased from the value depicted in Fig. 1 of 10°, while the value of θ/L and Re_x remained approximately constant, the separation point S moved upstream and the reattachment point R moved downstream. As the notch angle was decreased the opposite effect was observed, the separation point moved downstream and the reattachment point moved upstream. For the approaching flow conditions used in this investigation the separation point S was almost at the leading edge of the notch when the notch angle was greater than 16°, however, the separation point never did move completely down to the vertex of the notch, even when the notch angle was reduced to 7°.

The effect of a systematic change in the Mach number, particularly in the transonic regime with θ/L, Re_x, and notch angle constant is depicted in Figs. 3 and 5. These schlieren photographs clearly indicate that the separation point shifts as the Mach number is changed. The separation point was nearest the leading edge of the notch near a Mach number equal to one while for larger or smaller Mach numbers the separation point moved further downstream. The development of the shock wave and expansion wave structure for a v-notch is clearly visible if Fig. 5 for an increase through $M = 1$ while the effect of a change in notch angle on the shock wave-expansion structure is shown in Fig. 4.

The effect on the flow configuration when θ/L was changed while maintaining a constant Mach number, Re_x, and notch angle was not noticeable for the relatively small range of values of θ/L. Schlieren photographs were taken of the flow structure over four inch-long notches at a Mach number of two and the flow structures were identical to those shown in Fig. 2 even though θ/L was smaller by a factor of one-half.

2.2 Individual Flow Components

The basic flow model shown in Fig. 1 consists of various flow components whose relationships to the over-all flow model and to each other are pointed out in the following paragraphs.

i. Between sections (1) and (2) the boundary layer and external flow field expand around the initial corner of the notch. Analyses of this flow component were presented by Anandamurthy and Hammit (Ref. 1) and by White (Ref. 53).

ii. Between sections (2) and (3) the expanded shear layer develops along the surface and this can be analyzed using boundary layer integral techniques.

iii. From section (3) to section (4) the shear layer separates from the surface while the external flow changes direction, causing the separation shock. Analysis of this component might be accomplished by methods proposed in References 8, 13 and 36.

iv. The region between sections (4) and (5) consists of a developing free shear layer. Lamb (33) has presented a method for analyzing this type of flow. However, there is some concern as to whether Lamb's method will be adequate for this component since the free shear layer is in such close proximity to the wall. Lamb's method is based on the assumption of a quiescent wake, hence it neglects effects of wall interference.

v. Between sections (5) and (6) the flow reattaches to the surface while the external flow changes directions resulting in a reattachment shock. Several analyses of this component have been made and a critical discussion of these methods is presented by White (Ref. 53).

vi. From section (6) to section (7) the reattached shear layer begins to redevelop along the surface and boundary layer integral methods can be used to analyze the flow mechanism.

vii. The reattached shear layer and external flow field expand around the final corner of the notch between sections (7) and (8). This region is similar to that described in i), except that the approach shear layer is in the process of redevelopment after reattachment.

viii. Downstream of section (8) the shear layer undergoes further redevelopment along the flat surface.

The often unsatisfactory status of knowledge concerning the isolated flow components will be compounded by the complexity introduced through their internal interactions. On the other side, the delineation of the over-all model into components will permit an analysis, within limitations to be pointed out later in their quantitative and qualitative aspects.

Alternate methods of solving flow problems involving separation and reattachment based entirely on boundary layer concepts [Lees and Reeves (Ref. 34); Holden (Ref. 23)] can be subjected to criticism arising from the questionable validity of the basic boundary layer assumptions near separation and reattachment points.

3. DRAG FORCE ANALYSIS FOR THE V-NOTCH

3.1 Drag Coefficient for v-shaped Notches

The drag coefficient for a notch or groove is usually defined in one of the two ways, depending on the selection of a reference area. The most common definition which utilizes an area equal to the length times the width of the notch, the projected area on the plane surface, will be used as the definition of the drag coefficient and is given by equation (1).

$$C_d = \frac{D}{\frac{1}{2}\rho_e u_e^2 bL} \tag{1}$$

This is also a most convenient definition for the present case since the flat plate can be considered to be a v-notch with vanishing angle Ω.

3.2 Form Drag and Friction Drag

The drag force can be thought of as having two parts, drag due to shear forces and drag due to normal forces. The more common names are drag due to friction and pressure drag. The term pressure drag or form drag, is commonly used for subsonic flow, while the term wave drag is used in supersonic flow.

The form drag or wave drag is determined, within certain limitations arising from viscous interactions, by the geometry of the walls. The situation may change considerably however, when there is a region of separated flow such as exists in a v-shaped notch with the wall angle exceeding a limiting value which depends upon approach Mach number and the upstream boundary layer configuration. For this case the separation causes the pressure or wave drag to be strongly modified as a consequence of the actual flow geometry being at variance with wall boundary conditions. This is borne out by Fig. 6 where three different static pressure distributions are shown:

i. The theoretical wall pressure distribution for a supersonic flow (in absence of separation) due to Prandtl-Meyer expansions and a shock located at the vertex of the v-notch,
ii. the theoretical shock-expansion pressure distribution consistent with the flow model shown in Fig. 1, accounting for flow separation,
iii. experimental values obtained for the 10° v-shaped notch.

As noted before the measured pressure distribution differs greatly from curve i). As a consequence of separation the pressure increase at the center of the notch is eased by the interaction between the free stream with shear flow regions. Consequently, it can be recognized that the form or wave drag is not directly related to the wall geometry, but rather to the flow geometry as affected by separation. In comparing ii) to iii) it is also seen that the viscous layers by themselves are of major interest and also introduce an important modifying element to the theoretical shock-expansion model. The qualitative effect of the boundary layer when it is of significant thickness in comparison to the length of the notch is to reduce the drag force. For boundary layers that are thick relative to the notch dimension the notch is buried under the shear layer. The limiting case for this situation would be when the notch appears only as a surface imperfection for very thick boundary layers ($\delta/L \to \infty$).

3.3 Phenomenological Flow Model

The most significant difference between the inviscid and the actual flow configuration was recognized to be in the possible deviation of the streamlines from the geometry introduced by the solid walls. Consequently, the wave drag is no longer exclusively determined by the wall geometry, but instead, can be modified by the geometry of the separating and reattaching free shear layer. Because of this occurrence an attempt was made to examine the over-all drag force on the basis of a simplified, phenomenologically conceived model comprising the wave drag of the actual (separated) streamline configuration and those shear stresses contributed by the mixing shear layer. This concept should be reasonably correct as long as the shear force due to the attached boundary layers between sections (2) and (3) and between sections (6) and (7) in Fig. 1 remain small as compared to the form drag of the wall portions, which will not be the case for very shallow notches with vanishing separation regions. Such a model is shown schematically in Diagram 2.

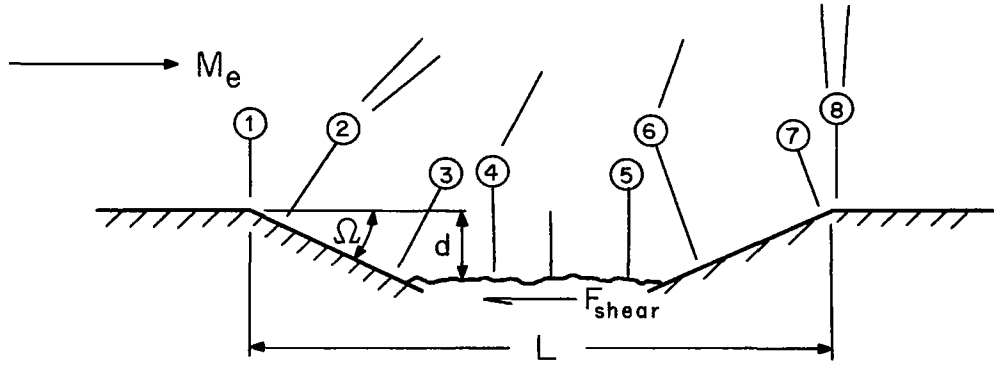

Diagram 2. Proposed Drag Force Model

It should be noted that the exact locations of either the separation point or the reattachment point are generally not known nor can they be determined presently by entirely analytical methods. However, for the present purpose it can be assumed that the separation streamline remains practically parallel to the external flow such that a single geometrical parameter, namely the penetration depth ratio d/r, fully describes the flow geometry of the model (the value d/r = 1 corresponds to the unseparated flow configuration). Since d/r is strongly dependent upon the already established parameters controlling the problem it will be treated as an undetermined quantity in the following theoretical analysis.

3.4 Utilization of the Flow Model

3.4.1 Linearized Theory for Supersonic Flow

For the restrictions that the Mach number is greater than unity (but not close to unity) and less than ten, linearized supersonic theory can be used to calculate the wave drag in the model. This calculation is an alternative to the shock-expansion method presented in the preceding section. For the actual configuration shown in Diagram 2 the drag force due to wave drag is given by (Ref. 46)

$$D_{wave} = \frac{1}{2} \rho_e u_e^2 bL \left(\frac{4}{\sqrt{M_e^2 - 1}} \right) \left(\frac{d}{L} \right) \tan (\Omega). \qquad (2)$$

The advantage of using linearized theory is that this relatively simple expression (eqn. 2) is found for the wave drag.

The drag force contribution of the separated shear layer is treated utilizing the method presented by Lamb (Ref. 33). Lamb analyzed theoretically the development of a two-dimensional free turbulent shear layer from an arbitrary initial velocity profile. The theoretical model for the developing free shear layer is shown in Diagram 3.

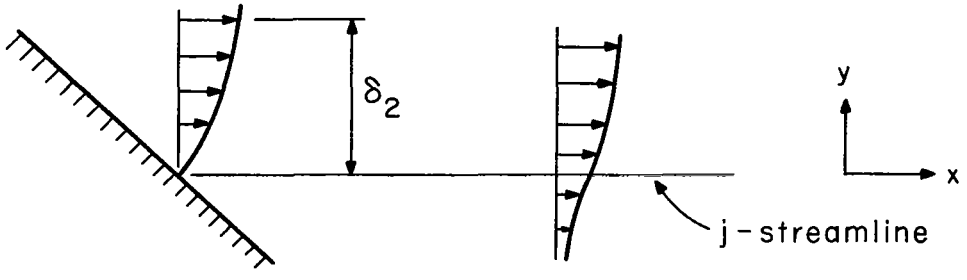

Diagram 3. Model for Developing Free Shear Layer

The drag force along the dividing streamline is given by

$$D_{mixing} = b\int_{o}^{x} \tau_j \, dx \tag{3}$$

Equation (3) can be rearranged to

$$D_{mixing} = \rho_e u_e^2 (1 - C_e^2)\delta_2 b\int_{o}^{\psi} J_j \, d\psi \tag{4}$$

where

$$\psi = \frac{x}{\delta_2}$$

and

$$J_j = \frac{\tau_j}{\rho_e u_e^2 (1 - C_e^2)} \tag{5}$$

Lamb shows that J_j is related to the integral $I_{j_{\eta_p}}$ by

$$J_j = \frac{d}{d\psi}\left(\frac{I_{j_{\eta_p}}}{\eta}\right) \quad . \tag{6}$$

Separating the variables in equation (6) and then integrating yields

$$I_{j_{\eta_p}} = \eta_p \int_o^{\psi} J_j \, d\psi \quad . \tag{7}$$

η_p is called the position parameter and is equal to $\frac{1}{2}\sqrt{\xi}$

where

$$\xi = \frac{1}{2\sigma^2} \int_o^{\psi} \psi f(\psi) \, d\psi .$$

The relationship between η_p and ψ was obtained by Lamb by applying the Navier -Stokes equations to the dividing streamline. The integral $I_{j_{\eta_p}}$ for the isoenergetic case is

$$I_{j_{\eta_p}} = \int_{-\infty}^{\eta_j} \frac{\phi^2}{1 - C_e^2 \phi_2} \, d\eta \tag{8}$$

where

$$\eta = \frac{y}{\delta_2} \eta_p$$

and

$$\phi = \frac{u}{u_e} = \phi(\phi_2, \eta, \eta_p)$$

where ϕ_2 is the initial velocity profile at separation. Substituting

from equation (7) into equation (4) yielded

$$D_{mixing} = \rho_e u_e^2 b(1 - C_e^2) \frac{\delta_2}{\eta} I_{j_{\eta_p}} \quad . \tag{9}$$

Adding D_{wave} and D_{mixing} and substituting this quantity into the expression for the notch drag coefficient [equation (1)] yields

$$C_d = \frac{2r}{L}\left[\frac{4}{\sqrt{M_e^2 - 1}}\left(\frac{d}{L}\right) + (1 - C_e^2)\frac{I_{j_{\eta_p}}}{\eta_p}\left(\frac{\delta_2}{L}\right)\left(\frac{1 - \frac{d}{r}}{1 - \frac{d}{L}}\right)\right] \tag{10}$$

Equation (10) was evaluated for various values of r/L and for representative values of δ_2 and C_e. The values of $I_{j_{\eta_p}}$ were calculated using the IBM 7094 digital computer operated by the Department of Computer Sciences at the University of Illinois.

It can easily be seen that, as $d/r \to 1$ there will be no contribution due to the shear drag of the mixing region and there is only the wave drag which now becomes

$$C_d = \left(\frac{2r}{L}\right)^2 \frac{4}{\sqrt{M_e^2 - 1}}$$

3.4.2 Shock-Expansion Theory

Restricting ourselves to the conditions of essentially non-separated flow ($d/r \square 1$) and considering only the wave drag, we express the drag coefficient (eqn. 1) in the form

$$C_d = \frac{\left(\frac{P_2}{P_1} - 1\right)\left(\frac{P_1}{P_e}\right)\left(\frac{r}{L}\right)}{\frac{K}{2} M_e^2} \qquad (11)$$

Calculations (using tabulated functions) have been made for a 7° v-notch and the results are plotted in Fig. 7 for a Mach number range of 1.33 to 2.0. The drag coefficient is evaluated only down to a Mach number of 1.33 because at this value for M_e and Ω = 7° the shock wave at the vertex of the notch is about to detach from the corner.

3.4.3 Special Features of the Transonic Problem

A simplified model for the analysis of the drag force of a v-notch can be constructed for the transonic flow regime (but with M_e greater than unity) if several assumptions are made. First, it is assumed that the notch angle is small (less than 10°) so that there is little if any separated flow near the vertex of the notch (hence d/r = 1). Secondly, it is assumed that wall shear drag (and mixing shear drag if present) is small as compared to wave drag. The flow model, which consists of a two-dimensional symmetrical v-shaped notch with an inviscid flow approaching the notch, is shown in Diagram 4.

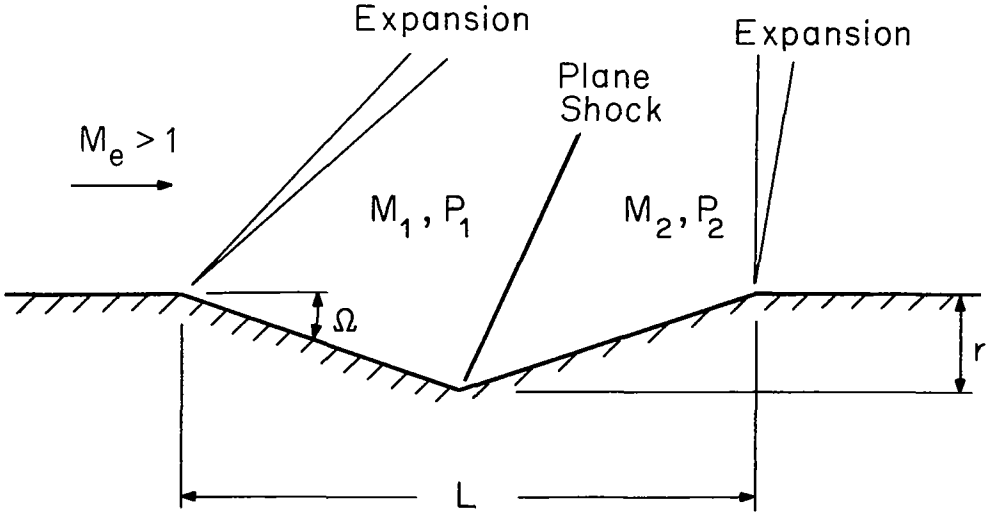

Diagram 4. Transonic Flow Model

The concept of this flow model is more clearly demonstrated if the change in the flow field is considered as M_e is decreased from a supersonic value of approximately two to unity. The drag coefficient for this notch is given by eqn. 11.

i) Mach Freeze Concept for Low Supersonic Approach Mach Number

For the example (3.4.2) previously considered ($\Omega = 7°$) when the approach Mach number is less than 1.33 the shock wave, which was assumed to be located at the vertex of the notch, must be detached from the vertex and located further upstream. This is exactly the phenomenon which can be observed in the photographs in Fig. 3. In order to facilitate the calculation of the drag coefficient in the region $1.0 < M_e < 1.33$ for a seven degree notch, the Mach number freeze concept first proposed by Bryson (Ref. 5) is used. The basis of this concept is that for free stream Mach numbers near one the local Mach number at a fixed location is approximately constant. When this concept is applied to this flow model the free stream Mach number, as far as the Mach freeze concept is concerned, is M_1 while the local Mach number is M_2. Then, assuming a constant Mach number M after the shock wave for M_e corresponding to 1.33 and $M_1 = 1.575$, the pressure ratio $P_2/P_{stag.}$ has a constant value. This must mean then, that the shock wave detaches from the vertex of the notch and changes the angle which it makes with the flow direction so as to give a constant value of $P_2/P_{stag.}$ as M_e decreases from 1.33 to 1.0. The drag coefficient calculated using the Mach freeze concept is also plotted in Fig. 7 for $1 < M_e < 1.33$.

ii) Transonic Similarity Relations

The correlation of drag coefficients in the transonic flow regime is generally done by utilizing the transonic similarity parameters, $\mathcal{J}$ and k.

$$k = \frac{M_e^2 - 1}{2\left(\frac{K+1}{2}\right)M_e^2\left(\frac{r}{L}\right)} \tag{12}$$

$$\mathcal{J} = \frac{C_d\left(\frac{K+1}{2}\right)^{1/3}}{\left(\frac{r}{L}\right)^{5/3}} \tag{13}$$

The similarity parameters k and $\mathcal{J}$ are obtained from the transonic similarity law (Ref. 46).

4. DRAG FORCE DUE TO BOUNDARY LAYER REHABILITATION DOWNSTREAM OF THE V-NOTCH

Part of the contribution to the drag force of a v-shaped notch is the increased skin friction on the flat surface downstream from the notch due to the redeveloping shear layer. As can bee seen in Figs. 2, 3, 4, and 5 there is nearly always a region of separated flow inside of the notch which causes a distorted (in comparison to the fully developed turbulent velocity profile) velocity profile at the end of the notch.

A prediction of the variation of the drag force in this region can be based on the concepts of boundary layer development within shear flow regions (Ref. 31) where this development is related to the shear layer development inside of the notch.

The limitations introduced by simplifying assumptions and the demonstrated need of experimental results for the extent of the separation region (penetration depth) and the uncertainties created by mutual interactions of flow components delineated in Section 2.2 stress the need for obtaining accurate experimental data. Such data are needed for gaining better insight into individual flow problems and interacting components, but most of all, to evaluate their composite effect on the over-all drag of v-shaped notches.

5. EXPERIMENTAL FACILITIES

5.1 Blowdown Wind Tunnels

The experimental work was carried out in the supersonic and transonic blowdown wind tunnel operated jointly by the Department of Mechanical and Industrial Engineering and the Department of Aeronautical Engineering. This tunnel is located in Aeronautical Laboratory B at the University of Illinois, Urbana, Illinois. The blowdown tunnel was supplied with air from a system of storage tanks with a total capacity of approximately 2500 cubic feet. The storage tank system was filled by using a 125 horsepower air compressor pumping up to a maximum pressure of 115 psig. Approximately one-half of an hour was required to fill the storage tank system to its capacity at 115 psig.

5.1.1 Supersonic

The supersonic test section had an area of 8 square inches and allowed observation through glass side windows and could be operated with stagnation pressures between 13 psig and approximately 60 psig. The stagnation temperature varied between 50 F and 90 F depending on the ambient conditions, stagnation pressure and run-time. The maximum run time for the supersonic tunnel was approximately four minutes for low stagnation pressures (less than 25 psig) and one minute for the higher stagnation pressures (greater than 35 psig). The test section Mach number was 1.96 but varied slightly with the stagnation pressure. At a stagnation pressure of about 30 psia and a stagnation temperature of 50 F the tunnel had a Reynolds number per foot of 9×10^6.

5.1.2 Transonic

A transonic test section with rectangular cross section was also used where the side walls consisted of glass plates suitable for optical studies while the top and bottom walls were slotted. For the purpose of the present investigation the slotted wall at the bottom was replaced by a solid wall into which the notch models or the balance carrying the drag models could be installed. The reduction in the wall permeability was permissible due to the small effective blockage effects of the models. The Mach number at the test section could be varied from approximately 0.5 to 1.2 by changing the tunnel stagnation pressure. No direct means of controlling the Reynolds number is possible in this range. The momentum thickness Reynolds number at the beginning of the test section varied from 7800 to 9500 for the stated Mach number variation. The maximum running time for the transonic test section was approximately one and one-half minutes at the higher Mach numbers ($1 \rightarrow 1.2$) and about three minutes at the lower (less than 0.9) Mach numbers.

5.2. Design of the Drag Force Balance

For the purpose of this study a drag force balance was designed and

constructed. A schematic diagram of the balance is shown in Fig. 8. The balance consists of a floating element with strain gages mounted on the flexure beams. Labyrinth seals are placed between the floating element and the balance base. A photograph of the drag balance is given as Fig. 10.

The drag force balance was extensively tested for preciseness and accuracy. A typical calibration curve is shown in Fig. 9. Many readings were taken to establish the curve and the data were repeatable to within ± ½%. The calibration curve was linear in this force range, as was expected, and passed through zero. The calibration constant, from the curve, was

$$\overline{K} = 0.1314 \text{ grams/dial unit.}$$

The drag force balance was also tested aerodynamically by using a flat plate model 4 inches long and 2.5 inches wide. This testing was conducted to determine three basic characteristics of the indicator:

i) accuracy
ii) plate misalignment effects
iii) effectiveness of the labyrinth seals.

5.2.1 Accuracy

Before the accuracy of the balance could be verified the boundary layer at the beginning of the flat plate had to be defined. Velocity traverses were made with a small probe (0.018 inches thick) on the floor of the tunnel at the beginning of the test section. The results of these traverses are shown in Table 1 and Fig. 11.

Fig. 11 is a plot indicating that the outer portion ($y/\delta > 0.3$) of the boundary layer did have a 1/7 slope and was representative of a fully developed compressible turbulent boundary layer.

Fig. 12 is a graphic comparison of the calculated (using integral techniques given in Ref. 27) Re_θ at the start of the flat plate model and the measured Re_θ at the same location as a function of stagnation pressure. Table 2 contains measured and calculated values at the beginning of the tunnel test section.

TABLE 1

SUPERSONIC TURBULENT BOUNDARY LAYER CHARACTERISTICS
AT THE BEGINNING OF THE TEST SECTION

P_o psia	δ in.	δ^* in.	θ in.	H	Re_x	Re_θ
34.0	0.147	0.035	0.0104	3.33	8.13×10^6	8855
39.95	0.147	0.0332	0.0099	3.34	8.36×10^6	9966
44.6	0.146	0.0324	0.0098	3.31	10.6×10^6	10944
49.4	0.144	0.031	0.00939	3.30	11.5×10^6	11685

TABLE 2

COMPARISON OF CALCULATED AND MEASURED BOUNDARY
LAYER QUANTITIES AT THE END OF THE SPLITTER PLATE

P_o	δ^*, in.		θ, in.		H	
psia	calc.	meas.	calc.	meas.	calc.	meas.
34.0	0.0306	0.035	0.0105	0.0104	2.91	3.33
39.95	0.0299	0.033	0.0103	0.0099	2.90	3.34
44.6	0.0291	0.0325	0.0101	0.0098	2.9	3.31
49.4	0.0286	0.0309	0.0099	0.0094	2.89	3.30

The results of the transonic velocity traverses were similar to those taken for supersonic flow and the velocity profiles had a shape similar to those for the supersonic regime. Re_θ at the beginning of the flat plate model is plotted in Fig. 13 and other data is given in Table 3.

TABLE 3

TRANSONIC BOUNDARY LAYER CHARACTERISTICS
AT THE BEGINNING OF THE TEST SECTION

M_e	θ, in.	δ^*, in.	H	Re_θ
0.606	0.023	0.0331	1.433	7920
0.91	0.0206	0.0346	1.683	9350
1.11	0.0156	0.0287	1.838	8530
1.24	0.0127	0.0242	1.902	8270

Flat plate drag coefficients have been plotted in Fig. 14 with $\overline{Re}_\theta$ as the abscissa. $\overline{C}_f$ is defined by

$$\overline{C}_f = \frac{\text{Drag Force}}{\frac{1}{2}\rho_e u_e^2 b(x_2 - x_1)} \tag{14}$$

and $\overline{Re}_\theta$ is define by

$$\overline{Re}_\theta = \frac{(Re_\theta)_1 + (Re_\theta)_2}{2} \tag{15}$$

Two curves are shown in Fig. 14 which are empirical equations for $\overline{C}_f$. The one labelled Culick-Hill-Howell was derived in Ref. 24 and is based on momentum-integral techniques. The curve labelled Spalding-Chi was obtained using results presented in Ref. (38). From these results it is seen that the accuracy of the measurements made by the balance are within reasonable limits.

5.2.2 Plate Misalignment Effects

Some tests were run with the drag balance where the flat plate model was intentionally misaligned with the balance base. The results of these tests showed that there was about a 10% deviation from the aligned value with approximately 0.003 inches misalignment. This deviation was somewhat less than that reported by O'Donnel and Westkaemper (Ref. 40) who reported about 16% deviation at 0.003 inches misalignment at a Mach number equal to two. The misalignment effects reported here however cannot be compared on an absolute basis to those reported by O'Donnel and Westkaemper because of the difference in the order of magnitude of the forces which were measured, but the qualitative effects were identical.

5.2.3. Effectiveness of the Labyrinth Seals

During the testing of the drag force balance several of the pressure distributions along the upstream and downstream faces were plotted in order to determine if the labyrinth seals were effective. The plots disclosed that if approximately 0.003 inches seal clearance were maintained then the pressure along the model faces was constant. Tests were run with and without the seals for the flat plate model and there was essentially no difference in the indicated drag force.

6. EXPERIMENTAL RESULTS

6.1 Separation Point Location

Several methods were used to locate the point of separation inside the v-shaped notches. Schlieren photographs were taken of the flow fields in supersonic and transonic flow for many of the v-shaped notches tested. From these photographs approximate separation locations were measured and recorded. Typical photographs are shown in Figs. 2, 3, 4, and 5.

For many of the notch shapes models were constructed with pressure taps (approximately 40) along the bottom of the notch so that static pressure distributions could be measured in the notch. A typical notch pressure distribution is shown in Fig. 6 for a two-inch, ten degrees notch with a free stream Mach number of 1.96. The approximate separation and reattachment points are also indicated in Fig. 6.

A third method that was used to locate the point of separation was the oil film technique. In this method a thin film of heavy oil (steam cylinder oil) was placed along the separating surface before the test. During the test a thin line of oil accumulated at the separation point. The location of this line was then recorded by observing its position relative to the pressure taps.

The results from all three methods are shown in Fig. 15 for a two-inch long notch. The individual results from the different techniques are not differentiated in Fig. 15 but the three methods were all in close agreement.

6.2. Drag Coefficient Measurements

6.2.1 Supersonic Drag Coefficients

For each of the notches tested two corrections were made to the indicated drag force. Diagram 5 depicts the forces acting on the model during the test.

$\overline{P}_u$ is the average pressure acting on the area A_g in the upstream model gap and $\overline{P}_d$ is the average pressure acting on the area A_g in the downstream model gap. The first correction term was that of the force, $F_{\Delta p}$, acting on the two model faces perpendicular to the free stream.

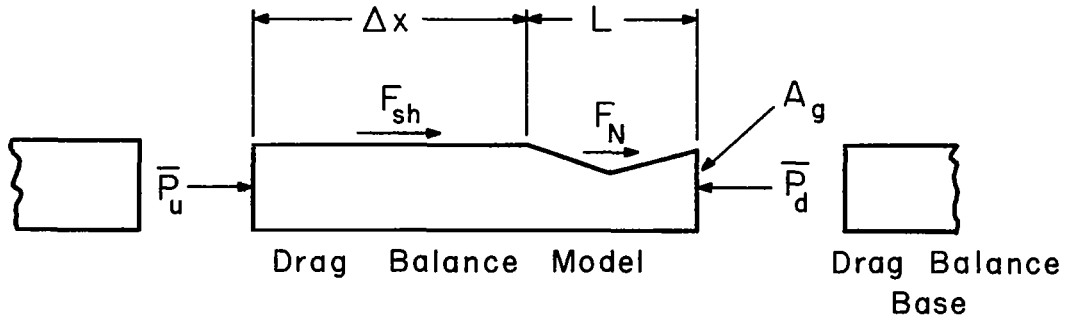

Diagram 5. Drag Force Correction Terms

$F_{\Delta p}$ is given by

$$F_{\Delta p} = (\bar{P}_u - \bar{P}_d)A_g \tag{16}$$

where A_g is the area over which the average pressures act. The second correction which was made to the indicated drag force reading accounted for the friction drag acting on the flat plate portion of the model. This correction term, F_{sh}, is given by

$$F_{sh} = \frac{1}{2} \rho_e u_e^2 \Delta x b \bar{C}_f \tag{17}$$

where $\bar{C}_f$ is the average drag force coefficient acting on the surface of length Δx.

The net drag force F_N of the notch then is given by

$$F_N = F_{balance} - F_{sh} - F_{\Delta p} \tag{18}$$

where $F_{balance}$ is the reading obtained from the drag force balance during the test.

For each model tested in the supersonic section the Reynolds number was the only quantity that could be varied. The results are plotted in Figs. 16, 17, 18, and 19 with the notch drag coefficient as the ordinate and the Re_θ number as the abscissa with notch length and angle as parameters. The effect of the shear layer thickness on the drag coefficient is depicted in Fig. 20.

6.2.2. Transonic Drag Coefficients

For the transonic tests the main variable was the Mach number and there was no direct control over the Reynolds number. The primary results, drag coefficient as a function of Mach number, are plotted in Figs. 24, 25, and 26 with notch length and notch angle as parameters. Fig. 32 shows the effects of the shear layer thickness, θ/L, on the drag coefficient with Mach number as a parameter.

6.3 Drag Force Test for Determining the Friction Drag of the Downstream Redevelopment

A series of tests were conducted in the supersonic test section in order to determine the influence of the notch on the friction drag force acting on the flat plate portion downstream from the notch. This effect was determined by placing the notch at different locations on the model in the drag force balance. For each test the same notch geometry was used but the notch was placed progressively further upstream for each test.

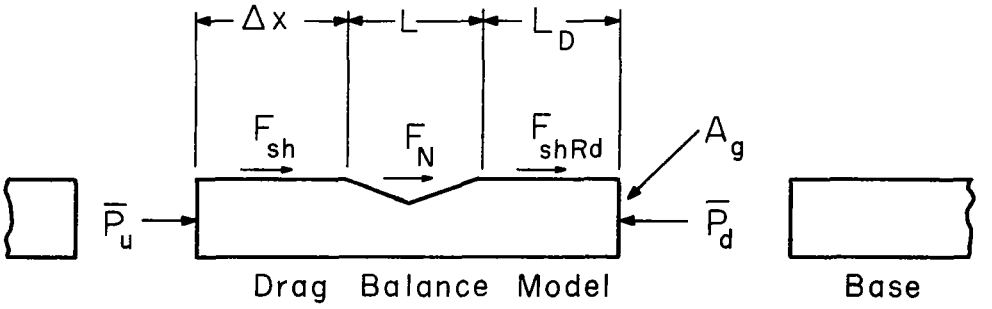

$$F_{sh} = \tfrac{1}{2}\rho_e u_e^2 \Delta x b \bar{c}_f$$

$$F_{\Delta p} = (\bar{P}_u - \bar{P}_d)A_g, \qquad F_N \text{ ◻ (experimental data)}$$

Diagram 6. Redevelopment Drag Force Correction Terms

Not only were the two corrections $F_{\Delta p}$ and F_{sh} made to the indicated drag force $F_{balance}$ as described in Part B above, but also the correction term for the drag force created by the notch was made. This additional correction term F_N is illustrated in Diagram 6 and its value was determined from the results obtained in the supersonic notch tests. The shear force F_{shRd}, on the flat surface of the model after the notch is given by

$$F_{shRd} = F_{balance} - F_{sh} - F_N - F_{\Delta p} \quad . \tag{19}$$

The results from this test are plotted in Fig. 33.

7. DISCUSSION OF RESULTS

The experimental results shown in Figs. 20 and 32 indicate that the Reynolds number effect is of minor importance when compared with the other variables. For the supersonic results shown in Fig. 20 it is clear that the notch angle is a significant factor in the determination of the drag coefficient for $\theta/L < 0.02$ while for $\theta/L > 0.02$ it is independent of the notch angle. A similar trend for transonic flow can be observed in Fig. 32, however, the value of θ/L where the drag coefficient becomes independent of notch angle is seen to be a function of Mach number. For this reason the results of this investigation are discussed, for any given Mach number, utilizing θ/L as the primary variable indicating the shear layer effect while the momentum thickness Reynolds number will be treated as a secondary variable.

For purposes of discussion a thin approaching boundary layer is one in which θ/L is small enough so that the notch angle affects the drag coefficient while a thick approaching boundary layer is one where the notch drag coefficient is independent of the notch angle. From Figs. 20 and 32 estimates of the values of θ/L for thin and thick boundary layers can be made. For $1.1 < M_e < 2$,

$$\left(\frac{\theta}{L}\right)_{thin} < 0.02 < \left(\frac{\theta}{L}\right)_{thick}$$

while for a subsonic Mach number of 0.6

$$\left(\frac{\theta}{L}\right)_{thin} < 0.09 < \left(\frac{\theta}{L}\right)_{thick}$$

7.1 Thin Approaching Boundary Layers

7.1.1 Supersonic Results, $M_e \simeq 2$

i) Reynolds Number Effect

All of the v-shaped notches tested in the supersonic ($M_e \simeq 1.95$) regime with thin approaching boundary layers exhibited an effect on the drag force coefficient for a

change in the Reynolds number. The notch drag coefficients for supersonic flow are plotted in Figs. 16, 17, and 18. In order to obtain a Reynolds number variation in the wind tunnel the stagnation pressure was varied. The change in stagnation pressure also caused a change in the momentum thickness of the boundary layer so that the effect shown in Figs. 16, 17, and 18 is a combined Reynolds number effect and shear layer thickness effect. In order to isolate the Reynolds number effect the data was replotted in Fig. 20 for constant values of the Reynolds number at various shear layer thicknesses. This figure indicates that for a constant shear layer thickness and notch angle the drag coefficient increases with increasing Reynolds number for thin approach boundary layers.

ii) Notch Angle Effect

The change in drag coefficient caused by a change in the notch angle can be most easily observed in Fig. 19. In the range of variables considered here (L = 3.5 inches, 2.25 inches, and 0.375 inch for thin boundary layers) the notch drag coefficient increased with increasing notch angle for a given notch length. Also shown in Fig. 19 are the drag coefficients estimated by using inviscid linearized supersonic theory for half-diamond-shaped profiles.

The progressive deviation of the drag coefficient from the linearized theory solution as the notch angle was increased demonstrated how the changing flow geometry reduced the drag coefficient from the theoretical solution based on the wall geometry.

A comparison of the experimental results with the solution obtained by using the proposed model for supersonic flow is shown in Fig. 22. The solid lines in Fig. 22 represent solutions of equation (10) using the proposed model and experimentally determined penetration depth ratios. The solid points in Fig. 22 are the experimental results for the drag coefficient for various notch lengths and angles. The agreement between the proposed model solution and the experimental results is satisfactory considering the assumptions which are made in the proposed model. The characteristic trends of the solution are interesting to note. For a given notch length the increase of the drag coefficient for an increase in notch angle above 13° is negligible because the flow separates close to the leading edge of the notch making the wave drag contribution small in comparison to the shear drag in the developing shear layer region. The effect of decreasing the notch angle for a given notch length is also demonstrated in Fig. 22. For very thin boundary layers ($\theta/L \simeq 0.003$ or L = 3.5 inches) the theoretical solution could be extrapolated to a maximum

penetration depth ($d/r \rightarrow 1$) indicating that for a long (3.5 inches) notch this would occur for a 6° notch angle. The relation to flat plate friction drag ($\Omega \rightarrow 0$) and to fully separated flow past a rectangular cutout (see Fig. 21) is shown in Fig. 23.

iii) Shear Layer Effect

For thin boundary layers there is an effect on the drag coefficient as the geometry of the notch is changed. Fig. 20 indicates that for each notch angle as the shear layer thickness was reduced the drag coefficient approached a constant value.

7.1.2. Transonic Results, M_e = 0.6 to 1.18

For the results obtained from the transonic flow regime the basic experimental parameters are different than they were in the supersonic regime. For these tests there was no direct control over the Reynolds number so that in this range of flow variables it was not possible to isolate the Reynolds number effect. However, this inability to establish the Reynolds number effect was not critical since as can be seen in Fig. 13, Re_θ had only a small variation between 7800 at M_e = 0.6 and 9100 at M_e = 0.09. The three basic effects considered in the transonic regime for thin boundary layers are notch angle, shear layer thickness, and Mach number.

i) Notch Angle Effect

For the case of a thin approaching boundary layer an increase in notch angle resulted in an increase in the drag coefficient for the range of values of Mach number tested. This was indicated by the results shown in Fig. 27 for a 2.25-inch long notch. The same results can be observed in Figs. 24, 25, and 26 for the 3.5-inch and 1-inch notches which are long enough to be in the thin boundary layer classification. For the lower Mach number range (0.6 to 0.8) the shorter notches (0.625- and 0.375-inch) are also in the thin approaching boundary layer classification (Fig. 32) and the same effect on the drag coefficient for a change in the notch angle is noted in Figs. 24, 25, and 26.

The transonic similarity parameters k and J were introduced as correlating parameters for the drag force coefficients. The experimental results from this investigation were plotted in terms of the parameters k and J in Figs. 29, 30, and 31. It can be noted from these figures that k and J are reasonable correlating parameters for thin approaching boundary layers.

ii) Shear Layer Effect

For the transonic flow regime the same qualitative effect for the approaching shear layer thickness on the notch drag coefficient was observed, however, the results also indicated that the value of the momentum boundary layer thickness for which the drag coefficient becomes independent of the notch angle increases for subsonic Mach numbers.

iii) Mach Number Effect

The Mach number effect observed in this investigation was the most pronounced effect and is illustrated in Figs. 24, 25, 26, and 27. It is obvious in Figs. 24, 25, and 26 that for v-notches a maximum value in C_d is going to occur for a Mach number greater than one and that the value of M_e where this maximum of C_d occurs is going to be dependent on the notch angle.

A model was proposed which qualitatively accounts for this shift in the maximum value of the drag coefficient near Mach number one. The Mach number at which the shock detaches in the v-notch is dependent upon the notch angle and this relationship is shown in Fig. 28. After the shock detaches from the vertex the Mach freeze concept proposed by Bryson (Section 3.4.3i) has been used to calculate the drag coefficient. The results from this calculation were shown in Fig. 7 for a 7° notch without separation and this curve has been replotted in Fig. 27 along with the experimental drag coefficients for a notch length of 2.25 inches. The qualitative agreement between the theory and experiment is good.

The theory and the experimental results do not agree quantitatively because in the actual flow case the flow separates from the surface causing the effective notch depth to decrease thus reducing the drag force coefficient. This change in the location of the separation point in passing through the transonic regime was shown in Figs. 4 and 5 for a 7° notch. This location of separation would cause the actual drag force coefficient to be reduced by about one-half which is the case shown in Fig. 27.

That this concept gives reasonable results well into the transonic flow regime is shown by the dashed curve in Fig. 27.

The value of the Mach number where the maximum drag coefficient occurs is estimated in Fig. 28. The quantity $(M_e)_{detach}$ is the theoretical Mach number in the free stream

when the shock detaches from the vertex of the notch.

7.2. Thick Approaching Boundary Layers

7.2.1. Supersonic Results, $M_e \simeq 2$

i) Reynolds Number Effect

For the thick boundary layer case (L = 0.375 inch and 0.625 inch) there was still an increase in C_d for an increase in Re_θ, however, the change was not as great as for the thin boundary layer case. The reason that this change is less is that the thicker approach boundary layer mollifies the effect of the notch on the free stream.

ii) Notch Angle Effect

The results of this investigation show that for thick approach boundary layers the notch angle has very little effect on the drag coefficient, in fact, the method of classification used assumed C_d to be independent of the notch angle in this regime.

iii) Shear Layer Effect

For the thick shear layers, as stated before, the boundary layer acted as a buffer region between the free stream and the solid boundaries with the net effect of reducing the drag coefficient. This reduction is quite obvious in Fig. 19 where, as θ/L was increased, the drag force coefficient was reduced.

7.2.2. Transonic Results, M_e = 0.6 to 1.18

i) Notch Angle Effect

The thick approaching boundary layer in the transonic flow regime eliminates the notch angle effect as can be noted in Figs. 24, 25, and 26 for L = 0.375 inch, and 0.625 inch. Similar results were observed in Figs. 29, 30, and 31 where the data were plotted in terms of k and J. For the thick boundary layers the transonic similarity parameters k and J also correlated the drag force coefficient data satisfactorily.

ii) Shear Layer Effect

For the supersonic Mach number range (M_e > 1.1) in the tran-

sonic flow regime the shear layer effects on the drag coefficient for the thick approaching boundary layers were identical to those for the thin boundary layers.

iii) Mach Number Effect

The Mach number effect for transonic thick approaching boundary layers was qualitatively the same as for the transonic thin approaching boundary layers.

7.3. Redeveloping Shear Layer Drag Downstream from the Notch

Tests were conducted to measure the effect that the v-notch has on the shear layer drag downstream from the notch. Experimental data representing the ratio of the measured drag force to the drag force on a flat surface equal to the redevelopment length at the same tunnel location but without the notch upstream are plotted in Fig. 33. Also shown in Fig. 33 is a theoretical estimate of the redeveloping shear layer drag assuming that the effective velocity at the start of the redevelopment region is 75% of the free stream velocity. The important conclusion from this series of tests is that there is a region of high frictional drag immediately behing the notch as a new boundary layer is developed within the shear flow layer present near the downstream corner of the v-notch, but that this high frictional drag decays to a fully developed boundary layer value within about four notch lengths downstream of the notch.

8. MISCELLANEOUS DRAG MEASUREMENTS OF RECTANGULAR AND CIRCULAR CAVITIES

Drag coefficients were measured for rectangular notches and circular cavities and these results are presented in Fig. 21. The drag coefficients for rectangular notches were strongly dependent upon the notch length and only slightly dependent upon the Reynolds number. The values of the drag coefficient measured here do not agree with those given by Charwat, Roos, Dewey, and Hitz (Ref. 9), (Diagram 7) which can only be partly explained by the fact that δ/r for these results was smaller by a factor of two than δ/r for their results.

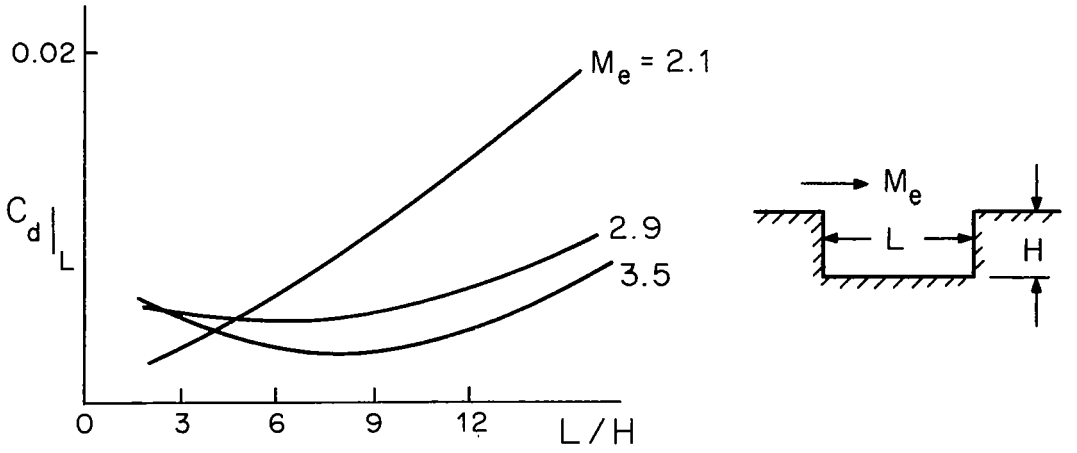

Diagram 7. Notch Drag Coefficients (Reference 9)

A circular cavity was likewise tested in the drag balance and also a theoretical calculation of the drag force was made using equation (9). The agreement is shown to be very good.

9. CONCLUDING REMARKS

From the analytical and experimental results of this investigation the following conclusions may be made about the drag coefficients for v-shaped notches.

i) The drag force on two-dimensional models can be accurately determined by direct force measurements using a newly developed balance employing strain gages. In particular, the effect of the notch angle at given values of Mach number and Reynolds number is shown to produce a continuous variation from flat plate friction drag values through combined wave drag and free jet mixing contribution to the shear drag in fully separated flow regions.

ii) The influences of the major experimental variables, namely notch geometry, flow Mach number and viscous effects (Reynolds number and boundary layer thickness ratio) could be established.

iii) A strong effect due to flow separation from the walls of v-shaped notches on the over-all flow configuration and drag forces (form drag and friction drag) was observed.

iv) The effect of the approaching boundary layer can be discussed in two categories, namely, thin or thick, depending on the degree to which the notch angle influences the value of the drag coefficient.

v) Reynolds number effects were generally small due to the large contribution of the free shear layer phenomena.

vi) Supersonic flow past v-notches with relatively thin approaching boundary layers can be analyzed on the basis of a simplified flow model accounting for the reduction in form drag by introducing information on the penetration depth ratio.

vii) Drag values obtained for transonic flow show an anomolous behavior near Mach number of unity in as much as they reach maximum values at slightly supersonic Mach numbers. This was found however, to be rationally explained by the "self-adjusting" configuration of the separation region.

viii) Theoretical analysis of the drag of shallow v-notches in the transonic flow regime using empirical information on the penetration depth ratio resulted in good quantitative agreement with measured values.

ix) The transonic parameters k and J are reasonable correlating quantities in the transonic flow regime for v-shaped notches.

x) The separation point inside of the v-shaped notch adjusts itself near Mach number equal to one resulting in an effective geometry change which reduces the expected notch drag coefficient.

BIBLIOGRAPHY

1. Anandamurthy, K. R., and Hammit, A. G., "Investigation of the Interaction of a Turbulent Boundary Layer with Prandtl, Meyer Expansion Fans at M = 1.88," Princeton University, AFOSR TN-58-839, Report No. 434, 1958.

2. Baronti, P. O., and Libby, P. A., "Velocity Profiles in Turbulent Compressible Boundary Layers," AIAA Journal, February, 1966, p. 193.

3. Bloom, M. H., and Rubin, S., "High Speed Viscous Corner Flow," JAS, Vol. No. 28, February 1961, p. 145.

4. Brinich, P. F., and Diaconis, N. S., "Boundary Layer Development and Skin Friction at Mach Number 3.05," NACA TN-2742, 1952.

5. Bryson, A. E., "An Experimental Investigation of Transonic Flow Past Two-Dimensional Wedge and Circular Arc Sections Using a Mach Zehnder Interferometer," NACA TN-2560, November, 1951.

6. Carrière, P., and Sirieix, M., "Facteurs D'influence du Recollement d'un Ecoulement Supersonique," ONERA Memo Technique No. 20, 1961.

7. Chapman, A. J., "Mixing Characteristics of a Free Jet Boundary with Consideration of Initial Boundary Layer Configuration," Ph.D. Thesis, Department of Mechanical Engineering, University of Illinois, 1953.

8. Chapman, D. R., Kuehn, D. M., and Larson, H. K., "Investigation of Separated Flows in Supersonic and Subsonic Streams with Emphasis on the Effect of Transition," NACA TN-3869, 1957.

9. Charwat, A. F., Roos, J. M., Dewey, F. C., and Hitz, J. A., "An Investigation of Separated Flows-Part I: The Pressure Field, and Part II: Flow in the Cavity and Heat Transfer," JAS, June 1961, July 1961, pp. 457, 513.

10. Chuan, R. L., "On the Supersonic Flow of a Viscous Fluid Over a Compression Corner," 1956 Heat Transfer and Fluid Mechanics Institute (pre-print), 1956, p. 185.

11. Coles, D., "Direct Measurement of Supersonic Skin Driction," JAS, Vol. 19, 1952, p. 717.

12. Coles, D., "Measurements of Turbulent Friction on a Smooth Flat Plate in Supersonic Flow," JAS, Vol. 21, 1954, p. 433.

13. Crocco, L., and Lees, L., "A Mixing Theory for the Interaction Between Dissipative Flows and Isentropic Streams," JAS, Vol. 19, 1952, p. 649.

14. Culick, F. E. C., and Hill, J. A. F., "A Turbulent Analog of the Stewartson-Illingworth Transformation," JAS, April 1958, p. 259.

15. Dailey, C. L., and Wood, F. C., Computation Curves for Compressible Fluid Problems, John Wiley & Sons, Inc., 1949.

16. Davies, P., Dyke, R. W., and Marchaj, C. A., "The Wind Tunnel Balances in the Large Low Speed Tunnel at Southampton University," University of Southampton Department of Aeronautics and Astronautics, Report No. 208, 1960.

17. Dhawan, Satish, "Direct Measurement of Skin Friction," NACA TN-2567, 1952.

18. Drougge, G., "An Experimental Investigation of the Influence of Strong Adverse Pressure Gradients on Turbulent Boundary Layers at Supersonic Speed," The Aeronautical Research Institute of Sweden, Report No. 46, 1953.

19. Erdos, J., and Pallone, A., "Shock-Boundary Layer Interactions and Flow Separation," Proceedings of the 1962 Heat Transfer and Fluid Mechanics Institute, pp. 239-255, 1962.

20. Golik, R. J., "On the Dissipative Mechanisms Within Separated Flow Regions," Ph.D. Thesis, Department of Mechanical Engineering, University of Illinois, 1962.

21. Hakkinen, R. J., "Measurements of Turbulent Skin Friction on a Flat Plate at Transonic Speeds," NACA TN-3486, 1955.

22. Hoerner, S. F., Fluid Dynamic Drag, Published by the author, 1958.

23. Holden, M. S., "An Analytical Study of Separated Flows Induced by Shock-Wave Boundary Layer Interaction," Cornell Aeronautical Report AI-1972-A-2, November 1965.

24. Howell, R. H., "Drag Forces of Two-Dimensional V-Shaped Notches in Transonic and Supersonic Turbulent Flow." Ph.D. Thesis, University of Illinois, Department of Mechanical Engineering, 1967.

25. Jackson, M. W., Czarnecki, K. R., and Monta, W. J., "Turbulent Skin Friction at High Reynolds Numbers and Low Supersonic Velocities," NASA TN-2687. 1965.

26. Kaye, J., "Survey of Friction Coefficients, Recovery Factors, and Heat Transfer Coefficients for Supersonic Flow," JAS, Vol. 21, 1954, p. 117.

27. Korst, H. H., "Approximate Calculations of Two-Dimensional Compressible Turbulent Boundary Layers with Pressure Gradient in the Free Stream," unpublished, 1958.

28. Korst, H. H., Page, R. H., and Childs, M. E., "Compressible Two-Dimensional Jet Mixing at Constant Pressure," University of Illinois, Engineering Experimental Station, M. E. Technical Note 392-1, 1954.

29. Korst, H. H., Chow, W. L., and Zumwalt, G. W., "Research on Transonic and Supersonic Flow of Real Fluids at Abrupt Increases in Cross Section," University of Illinois, ME Technical Report 392-5, Second Edition, October 1964.

30. Korst, H. H., and Chow, W. L., "Non-Isoenergetic Turbulent (Pr_t = 1) Jet Mixing Between Two Compressible Streams at Constant Pressure," University of Illinois, ME TN-393-2, April 1965.

31. Korst, H. H., "Dynamics and Thermodynamics of Separated Flows," Repring from Single and Multi-Flow Processes (Symposium of Rutgers Engineering Centennial), Rutgers University Press, 1965.

32. Krishnamurty, K., "Acoustic Radiation from Two-Dimensional Rectangular Cutouts in Aerodynamic Surfaces," NACA-TN-3487, 1955.

33. Lamb, J. P., "The Development of Free Turbulent Shear Layers," Rocket Test Facility, Arnold Engineering Development Center, AEDC-TR-65-184, 1965.

34. Lees, L., and Reeves, B. L., "Supersonic Separated and Reattaching Laminar Flows: I. General Theory and Application to Adiabatic Boundary-Layer/Shock-Wave Interactions," AIAA Journal, Vol. 2, 1964, p. 1907.

35. Liepmann, H. W., and Bryson, A. E., "Transonic Flow Past Wedge Sections," JAS, December 1950, p. 745.

36. Mager, A., "On the Model of the Free, Shock-Separated, Turbulent Boundary Layer," Journal of the Aeronautical Sciences, Vol. 23, 1956, pp. 181-184.

37. Murray, W. M., and Stein, P. K., Strain Gage Techniques, Massachusetts Institute of Technology Press, 1958.

38. Neal, L. Jr., and Bertram, M. H., "Turbulent-Skin Friction and Heat Transfer Charts Adapted from the Spalding and Chi Method," NASA-TN-D-3969, 1967.

39. O'Donnel, R. M., "Experimental Investigation at a Mach Number of 2.41 of Average Skin Friction Coefficients and Velocity Profiles for Laminar and Turbulent Boundary Layers and an Assessment of Profe Effects," NACA TN-3122, 1954.

40. O'Donnel, F. B., and Westkaemper, J. C., "Measurement of Errors Caused by Misalignment of Floating Element Skin Friction Balances," AIAA Journal, Vol. 3, 1963.

41. Perry, C. C., and Lissner, H. R., The Strain Gage Primer, McGraw-Hill Book Co., Inc., 1955.

42. Peterson, J. B., "A Comparison of Experimental and Theoretical Results for the Compressible Turbulent Boundary Layer Friction with Zero Pressure Gradient," NACA TN-D-1795, 1963.

43. Roshko, A., "Some Measurements of Flow in a Rectangular Cutout," NACA TN-3488, 1955.

44. Schick, W. F., "A Floating Element Wind Tunnel Balance," University of California Institute of Engineering Research Series No. 20, Technical Report H. E.-150-159, 1958.

45. Schlichting, H., Boundary Layer Theory, McGraw-Hill Book Company, Inc., Fourth Edition, 1960.

46. Shapiro, A. H., The Dynamics and Thermodynamics of Compressible Fluid Flow, Volumes I and II, The Ronald Press Company, 1954.

47. Sommer, S. C., and Short, B. J., "Free Flight Measurements of Turbulent Boundary Layer Skin Friction in the Presence of Severe Aerodynamic Heating at Mach Numbers from 2.8 to 7.0," NACA TN-3391, 1955.

48. Spreiter, J. R., "On the Application of Transonic Similarity Rules," NACA TN-2726, 1952.

49. Steiger, M. H., and Bloom, M. H., "Linearized Viscous Free Mixing with Streamwise Pressure Gradients," AIAA Journal, Vol. 2, February 1964, p. 263.

50. Thomke, G. J., "Separation and Reattachment of Supersonic Turbulent Boundary Layers Behind Downstream Facing Steps and Over Cavities," Douglas Report SM-43062, Douglas Aircraft Co., 1964.

51. Truckenbrodt, E., "A Method of Quadrature for Calculation of the Laminar and Turbulent Boundary Layer in the Case of Plane and Rotationally Symmetrical Flow," NACA TN-1379, 1955.

52. Vollus, R. J., Handbook of Supersonic Aerodynamics--Section 20--Wind Tunnel Instrumentation and Operation, NAVORD Report 1488, Volume 6, 1961.

53. White, R. A., "Turbulent Boundary Layer Separation from Smooth-Convex Surfaces in Supersonic Two-Dimensional Flow." Ph.d. Thesis, University of Illinois, Department of Mechanical Engineering, 1963.

54. Wilson, R. E., "Turbulent Boundary Layer Characteristics at Supersonic Speeds--Theorty and Experiment," JAS, Vol. 17, 1960, p. 585.

55. Wuerer, J. E., and Clayton, F. I., "Flow Separation in High Speed Flight A Review of the State of the Art," Douglas Aircraft Company, Inc., Douglas Report SM-46429, 1965.

LIST OF FIGURES

LIST OF FIGURES (CONTINUED)

$\Omega = 10^{\circ}$ $M_e = 1.96$ $\delta_1 = 0.18$ in.

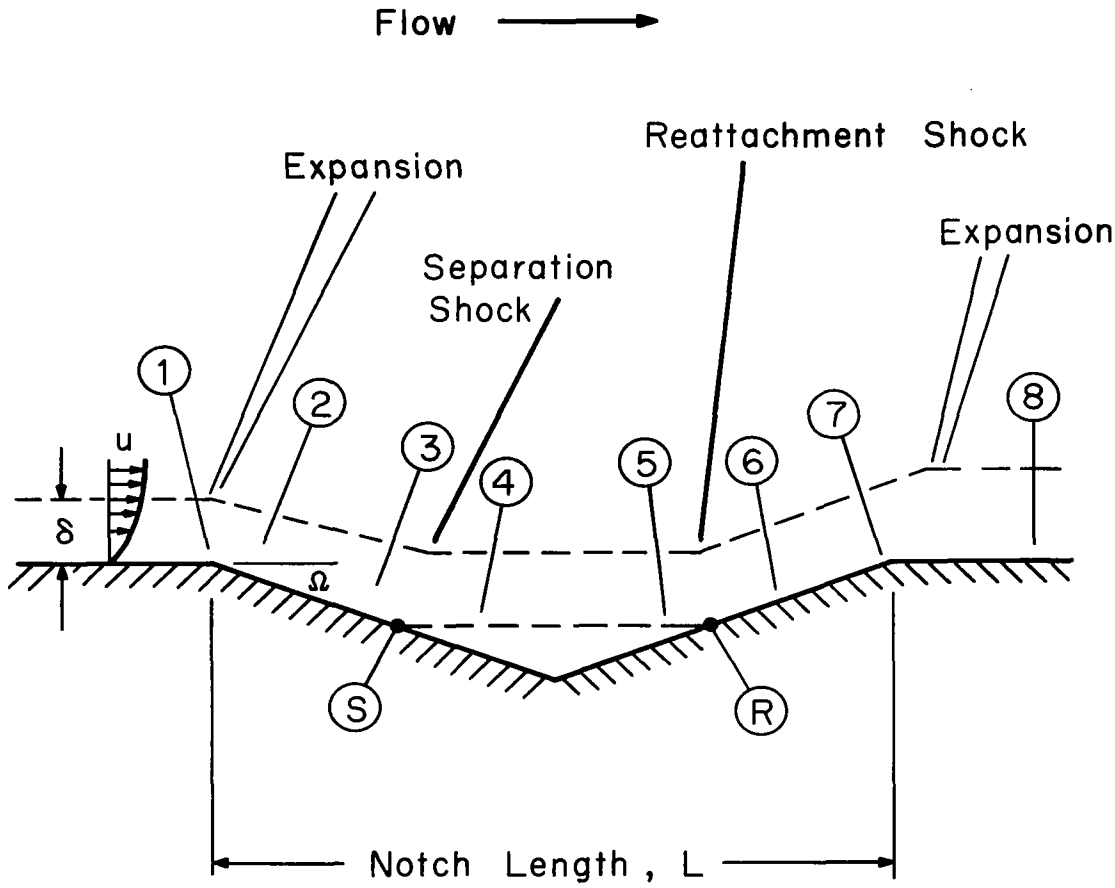

Figure 1. Theoretical Supersonic Flow Model

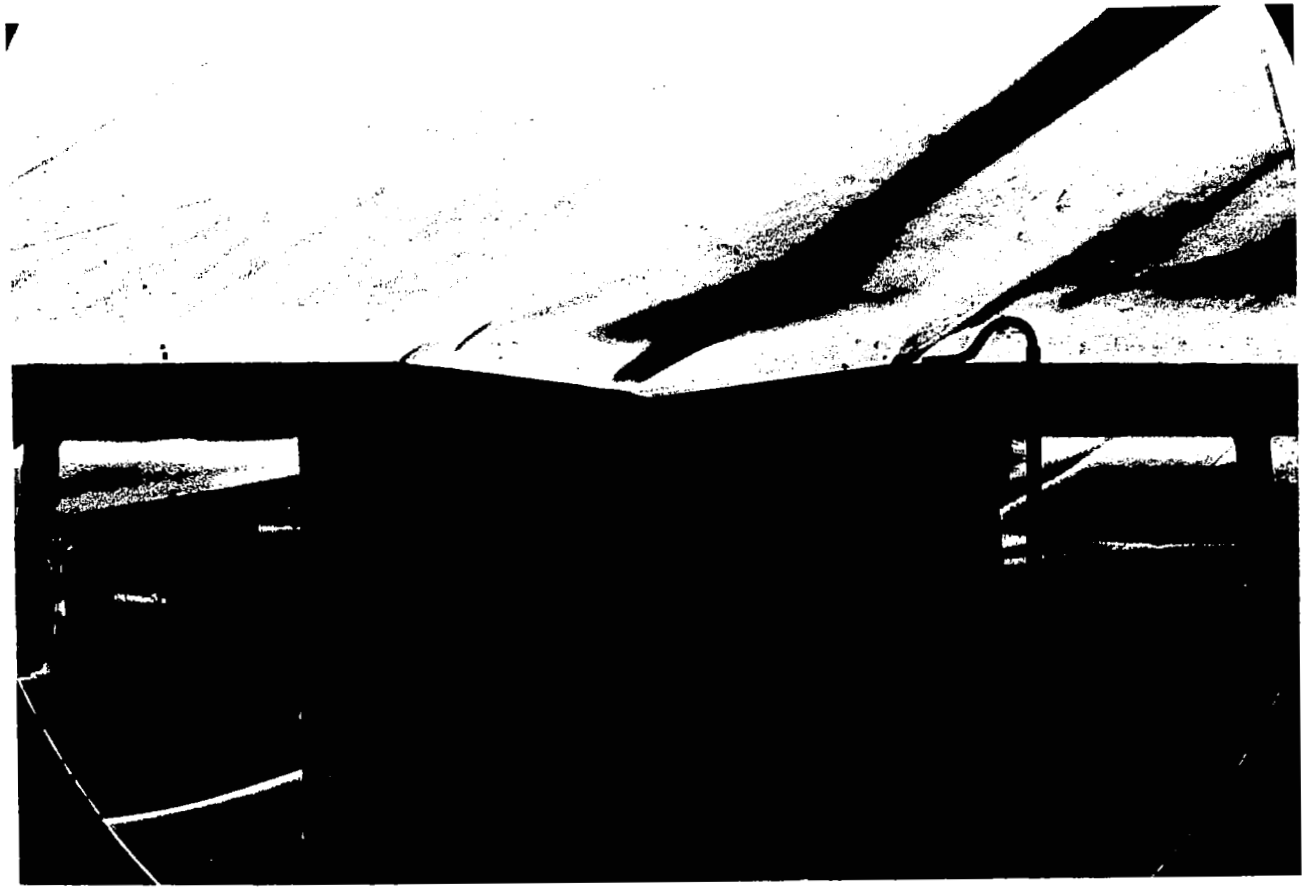

Figure 2(a). Supersonic Notch Flow (M_e = 1.96, Ω = 7°, L = 2 in.)

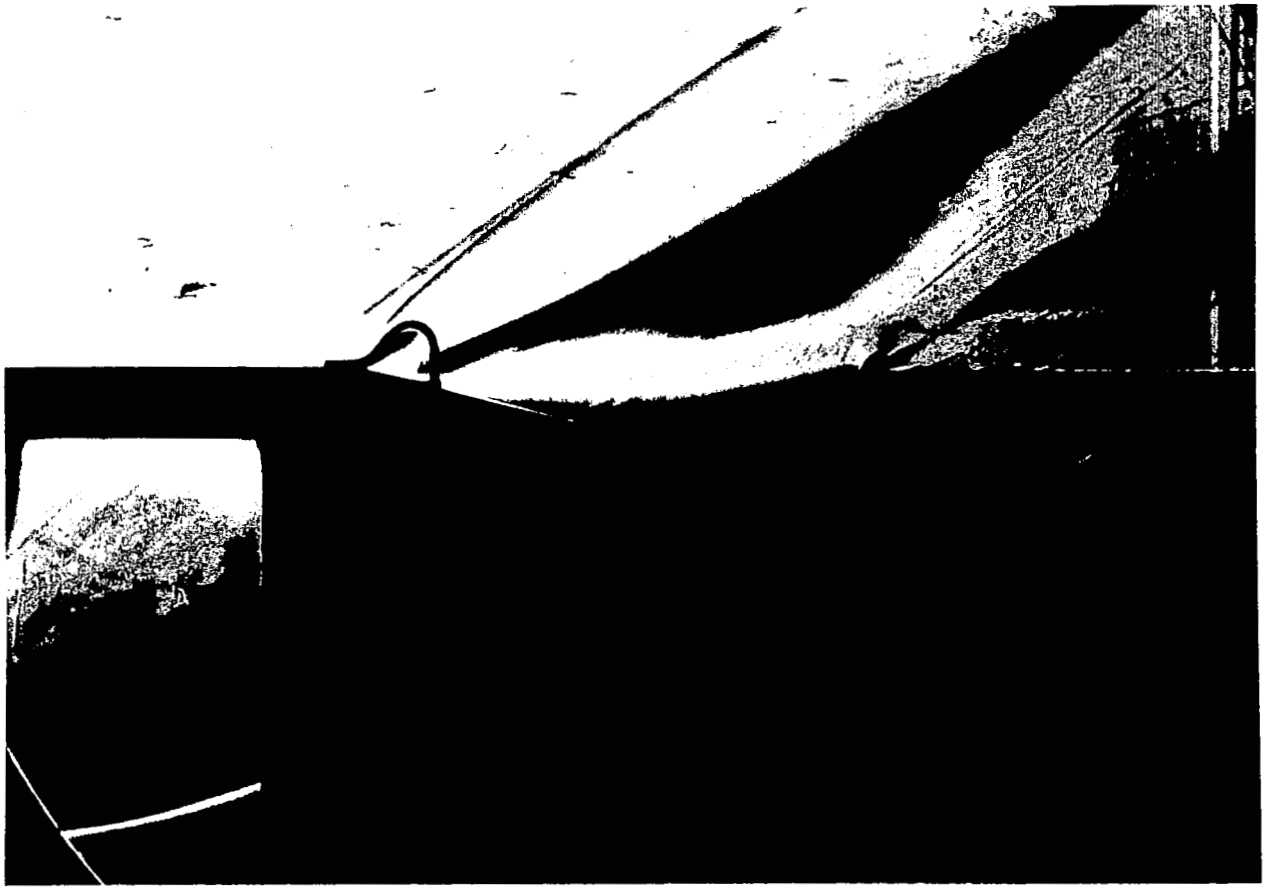

Figure 2(b). Supersonic Notch Flow (M_e = 1.96, Ω = 13°, L = 2 in.)

Figure 2(c). Supersonic Notch Flow (M_e = 1.96, Ω = 16°, L = 2 in.)

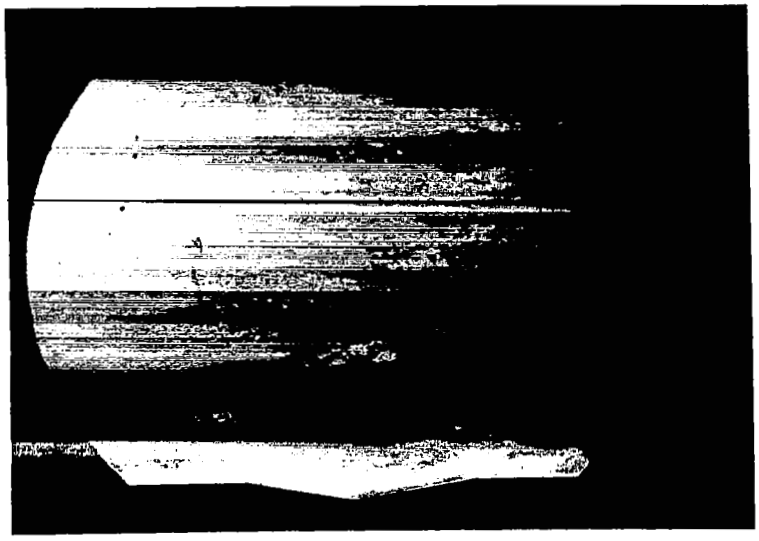

(a) M_e = 0.6, L = 2 in., Ω = 10°

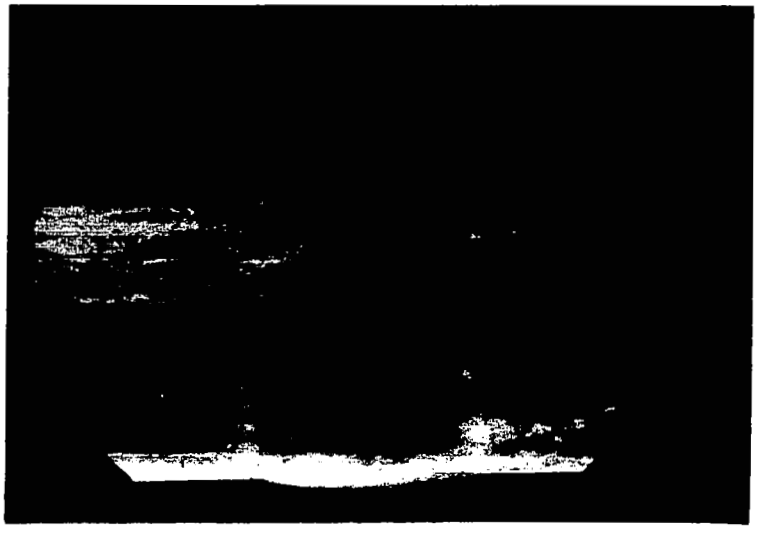

(b) M_e = 0.9, L = 2 in., Ω = 10°

Figure 3. Transonic Flow Over Notch

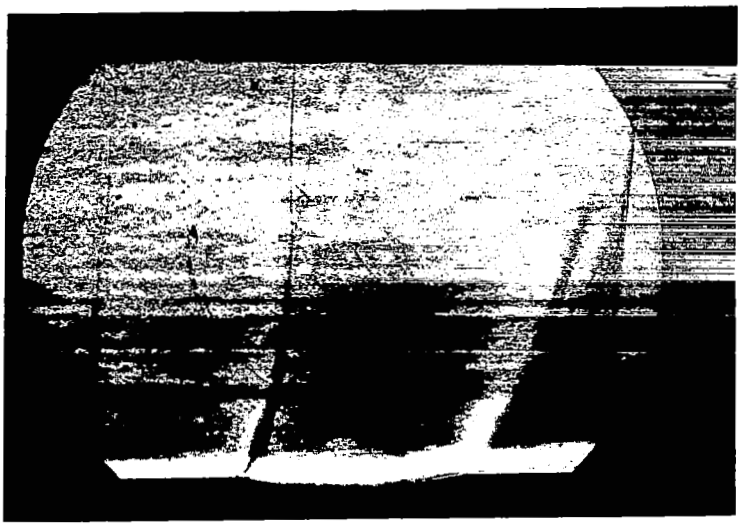

(c) M_e = 0.98, L = 2 in., Ω = 10°

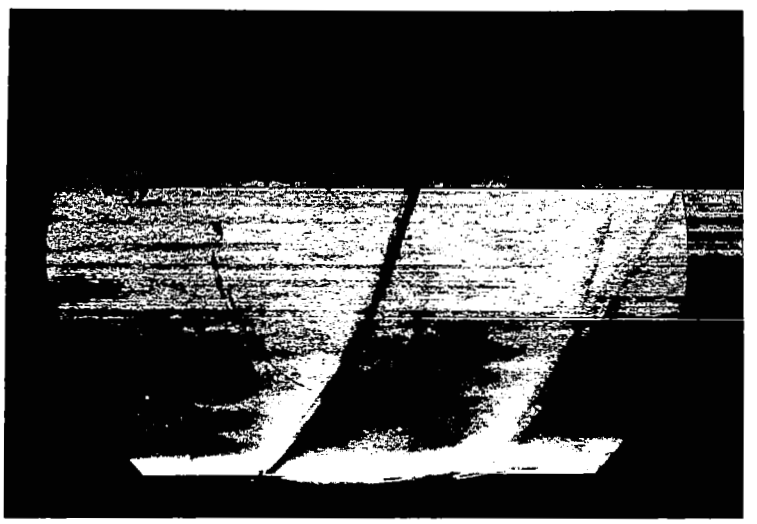

(d) M_e = 1.09, L = 2 in., Ω = 10°

Figure 3. Transonic Flow Over Notch (continued)

(a) M_e = 1.14, L = 2 in., Ω = 7°

(b) M_e = 1.14, L = 2 in., Ω = 10°

Figure 4. Transonic Flow Over Notch

(c) M_e = 1.14, L = 2 in., Ω = 13°

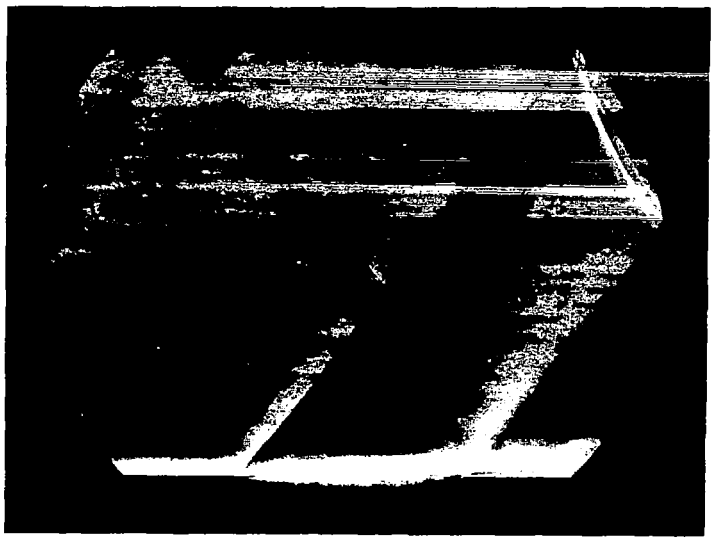

(d) M_e = 1.14, L = 2 in., Ω = 16°

Figure 4. Transonic Flow Over Notch (continued)

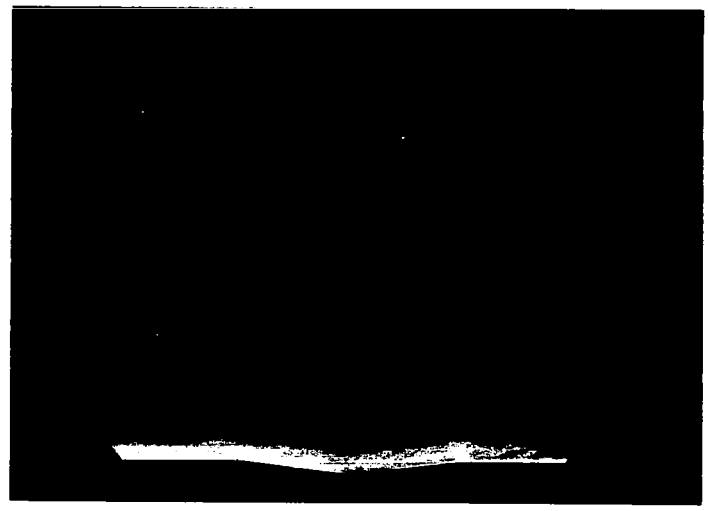

(a) M_e = 0.61, L = 2 in., Ω = 7°

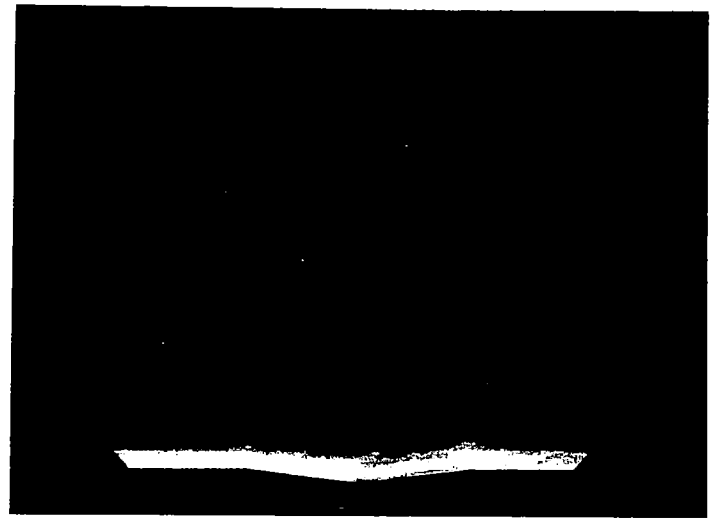

(b) M_e = 0.83, L = 2 in., Ω = 7°

Figure 5. Transonic Flow Over Notch

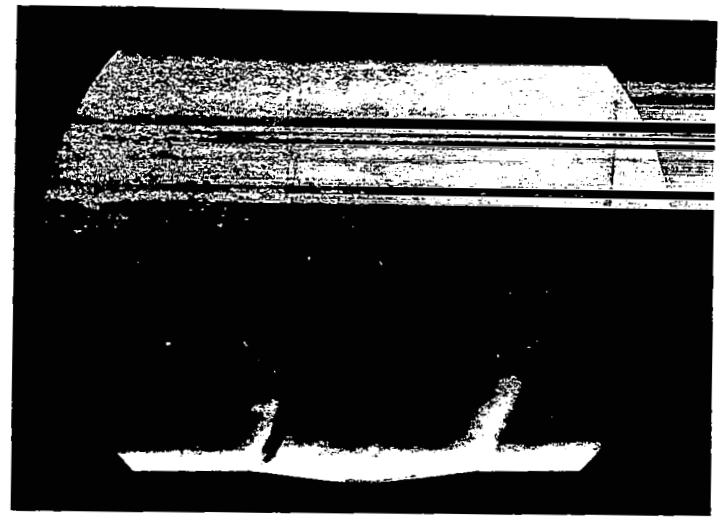

(c) M_e = 0.99, L = 2 in., Ω = 7°

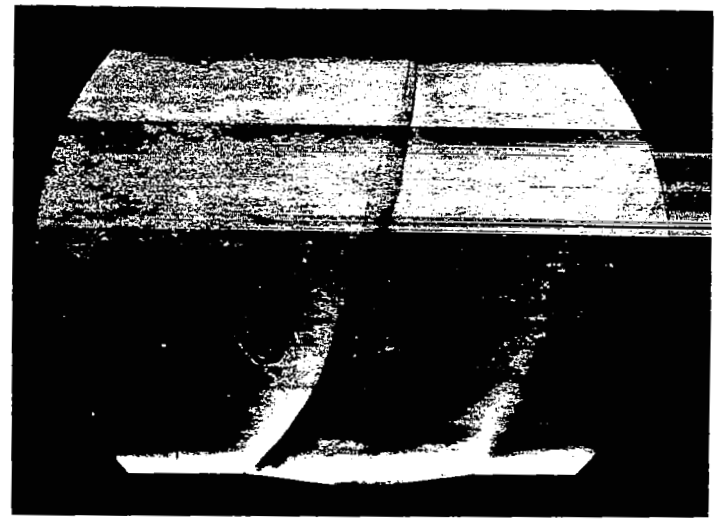

(d) M_e = 1.09, L = 2 in., Ω = 7°

Figure 5. Transonic Flow Over Notch (continued)

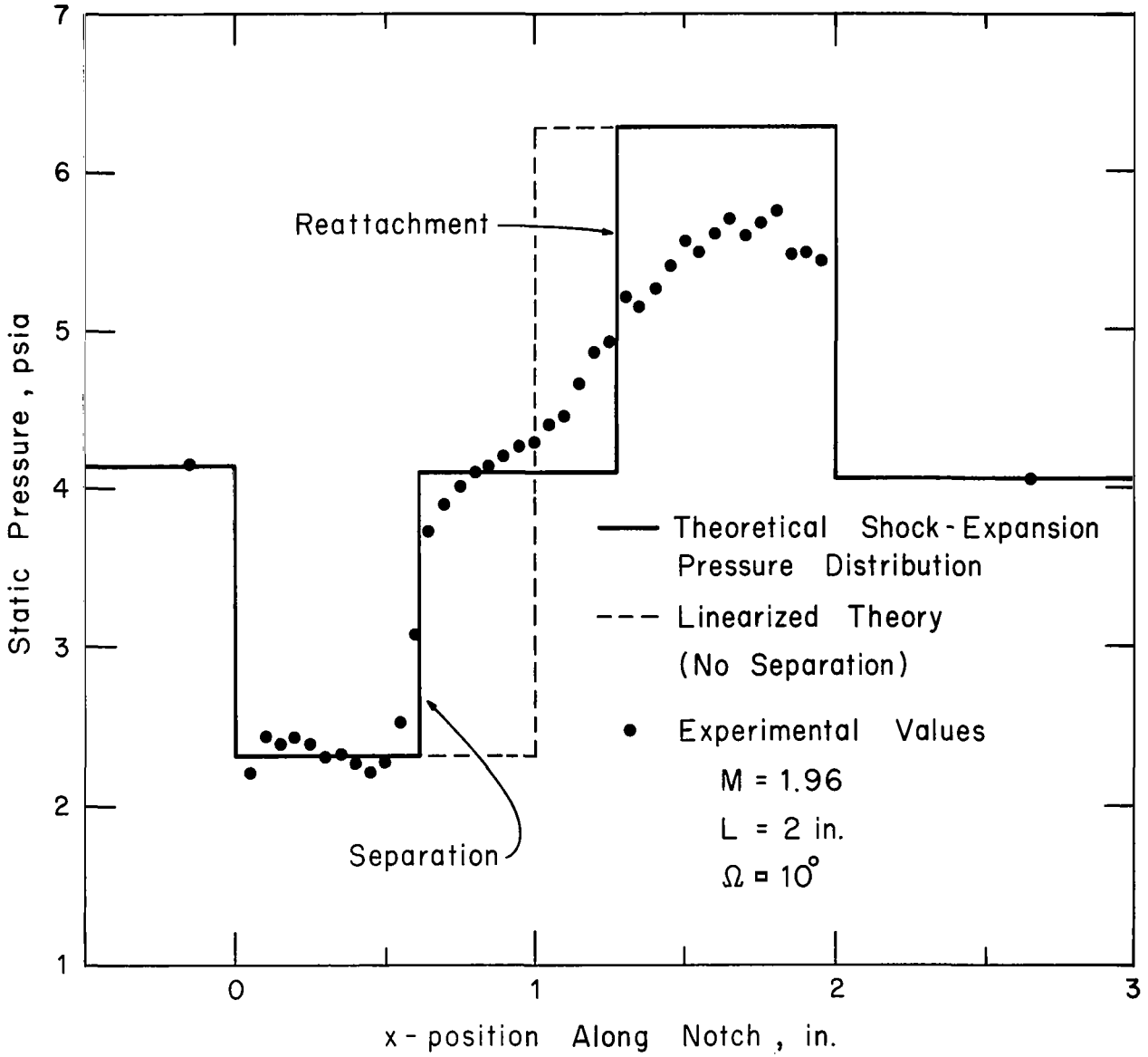

Figure 6. v-notch Pressure Distribution

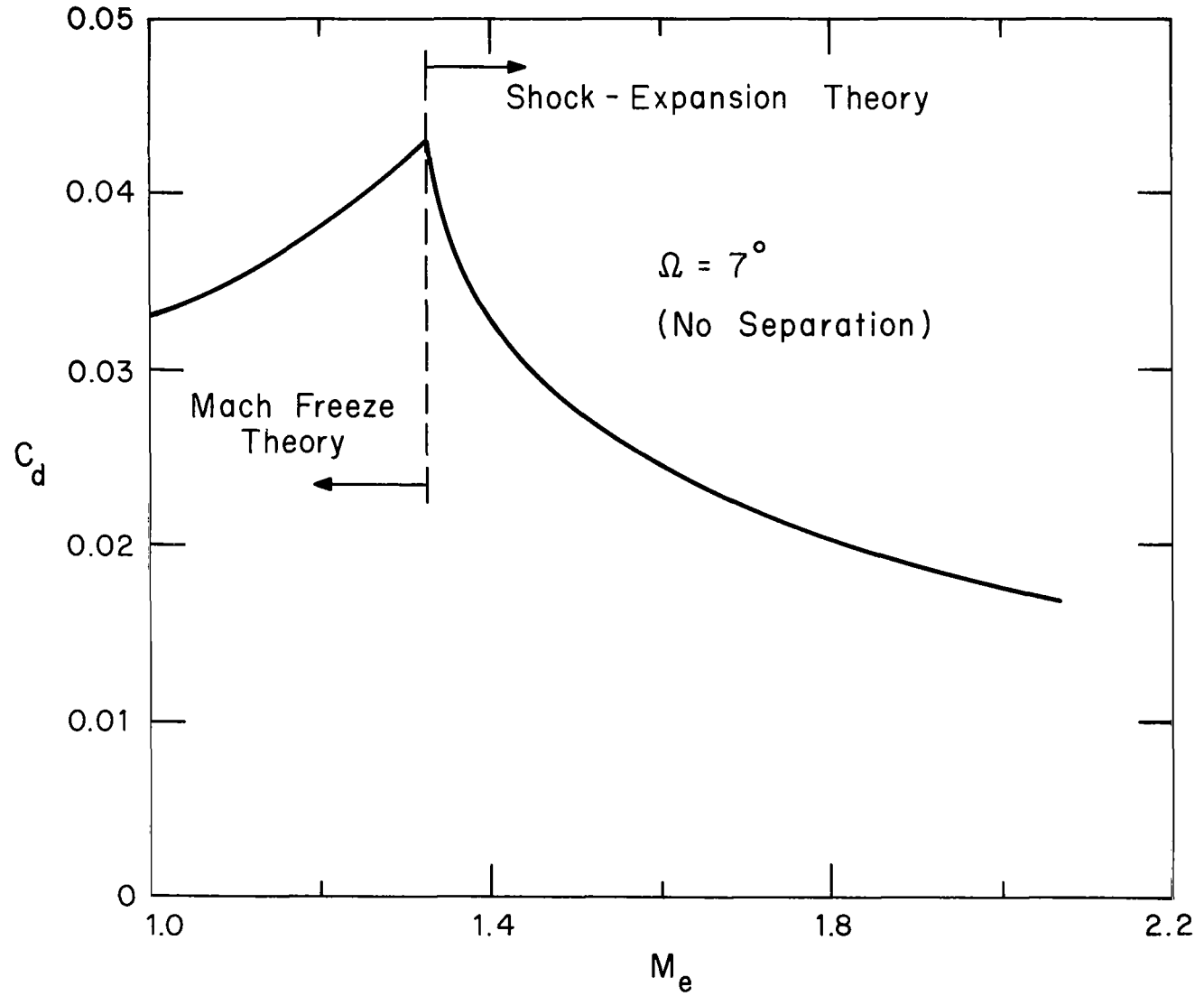

Figure 7. Transonic Flow Model C_d Variation

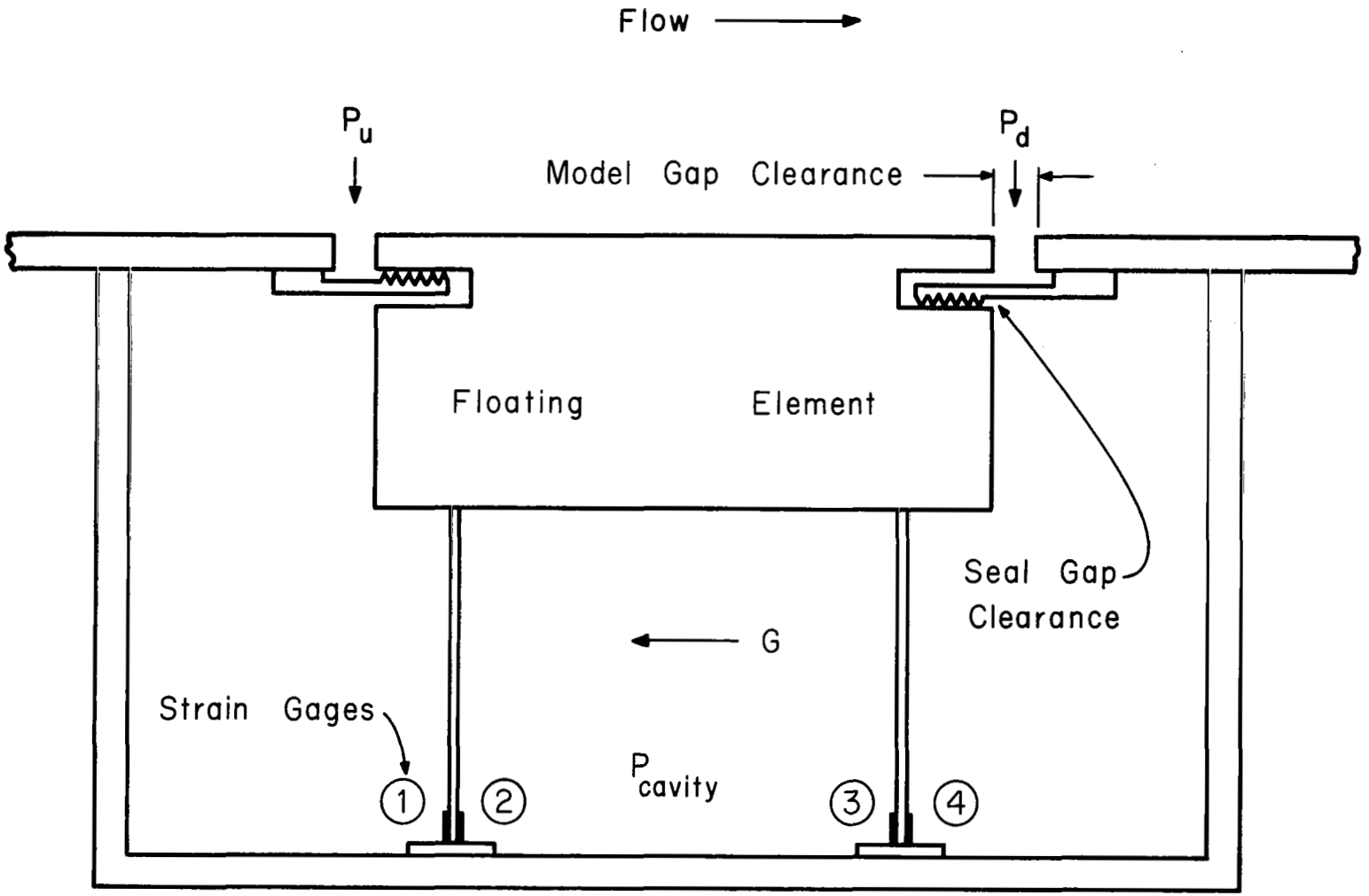

Figure 8. Diagrammatic Drawing of Drag Force Balance

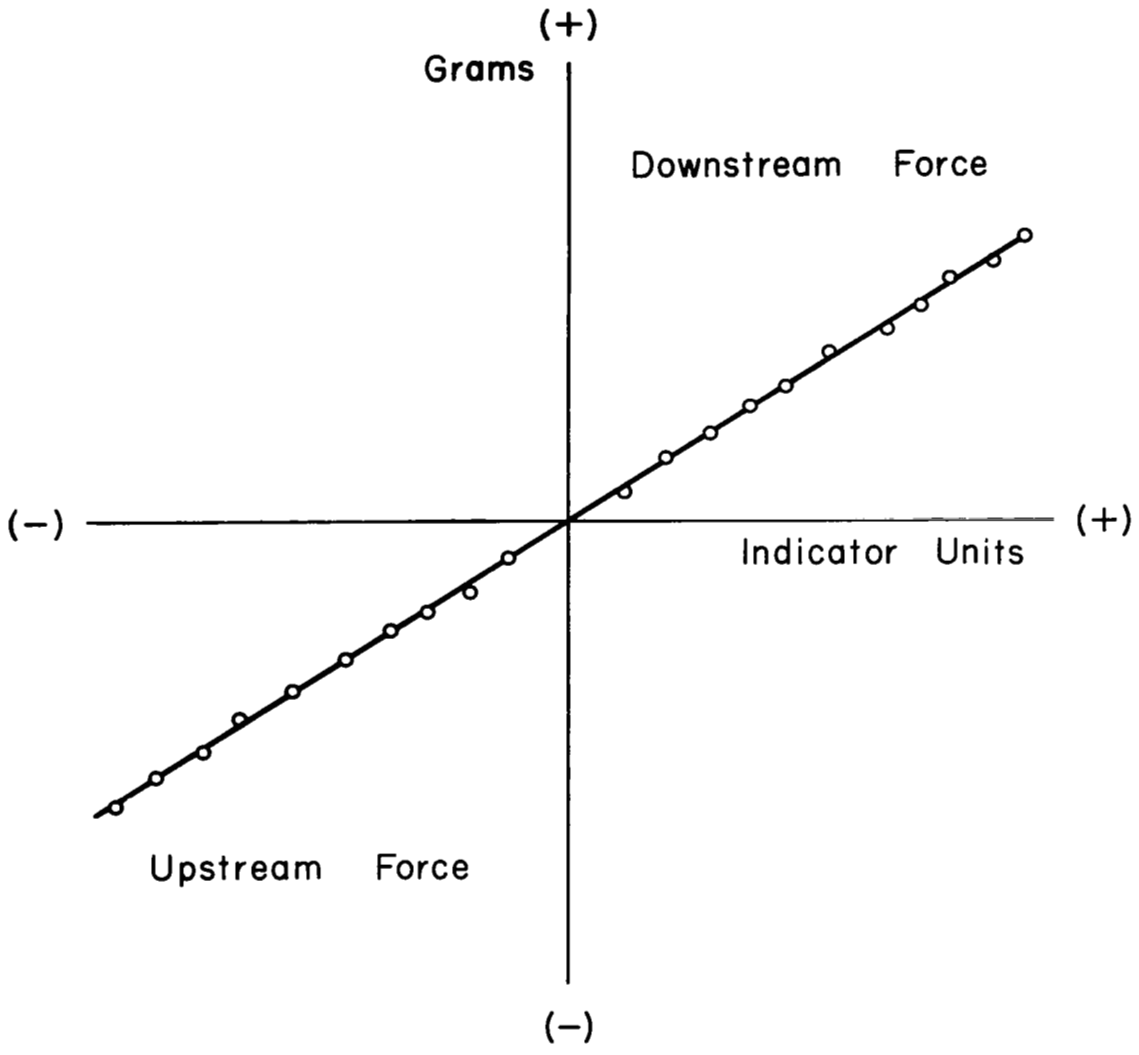

Slope = 0.1314 gram/unit
Gain = 20
Gage Factor = 2.12

Figure 9. Drag Balance Calibration

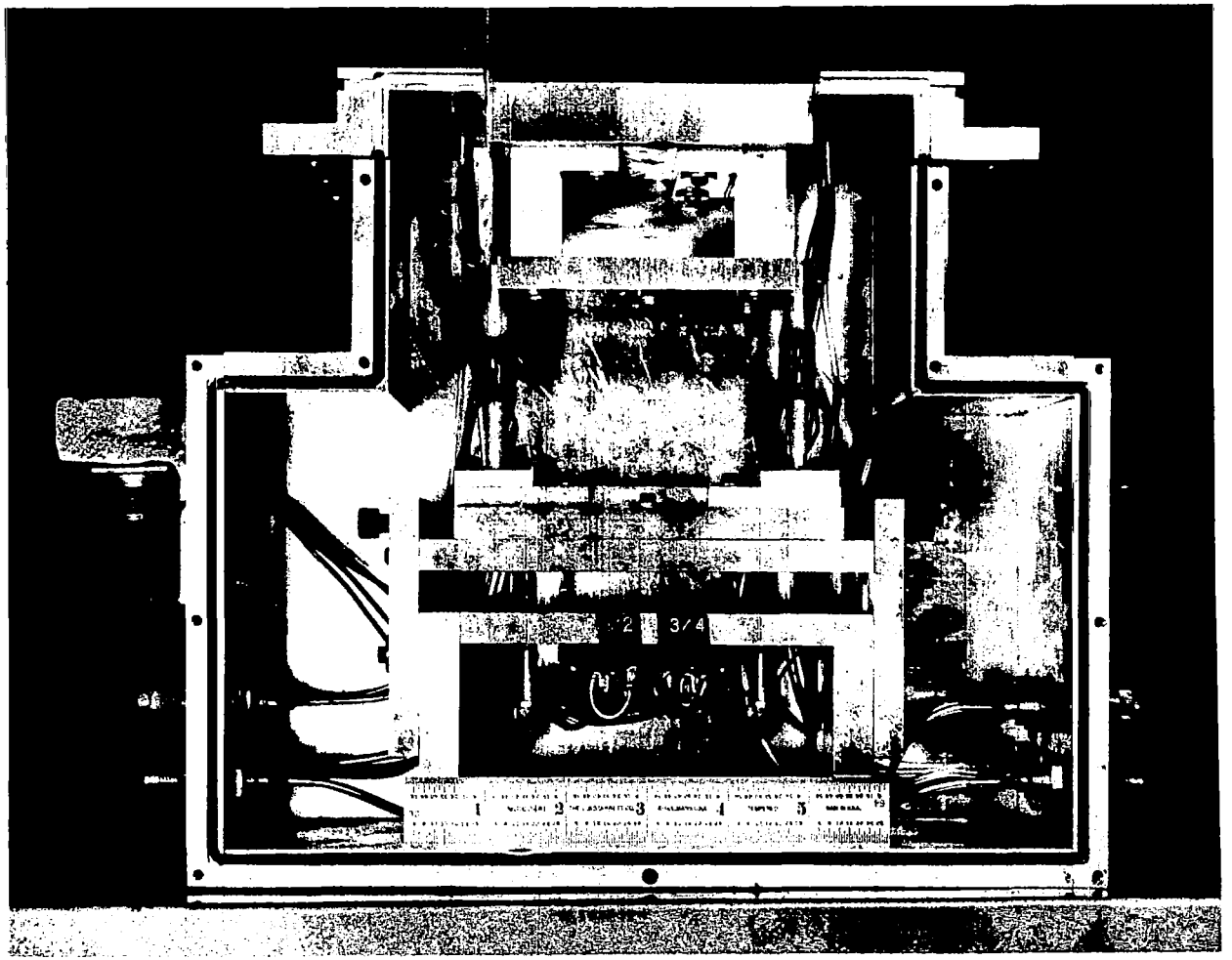

Figure 10. Drag Force Balance

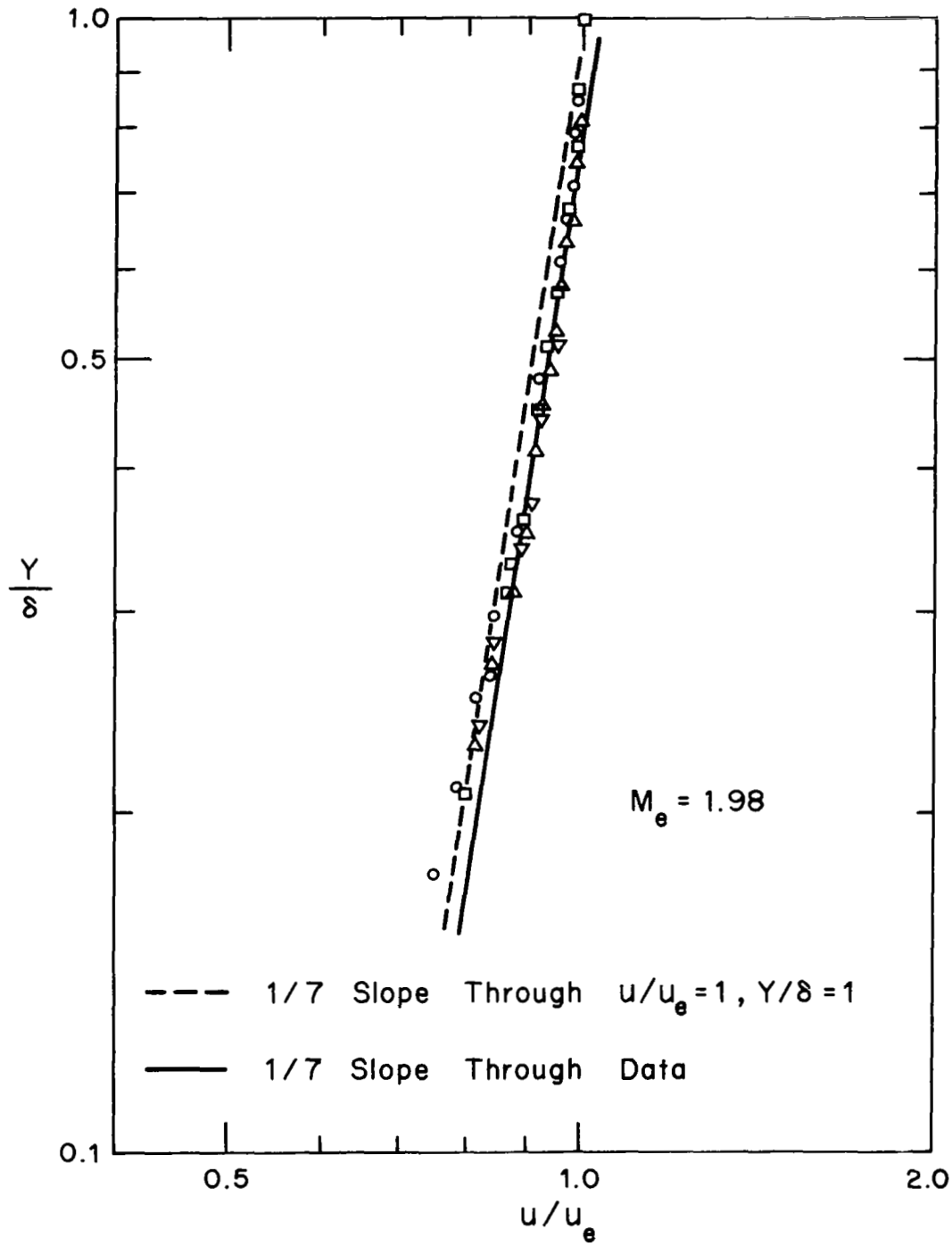

Figure 11. Supersonic Velocity Traverse Results

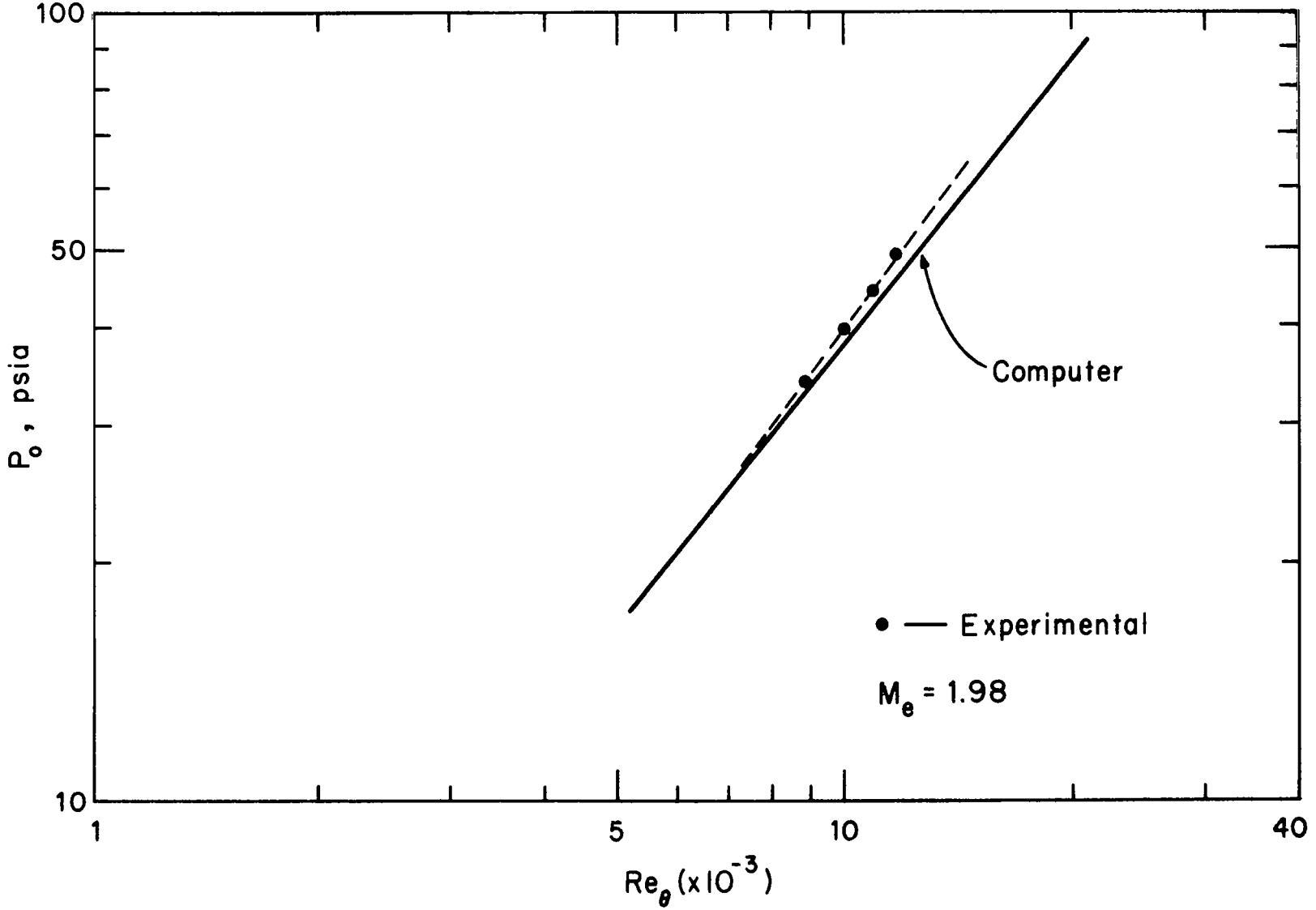

Figure 12. Momentum Thickness Reynolds Number

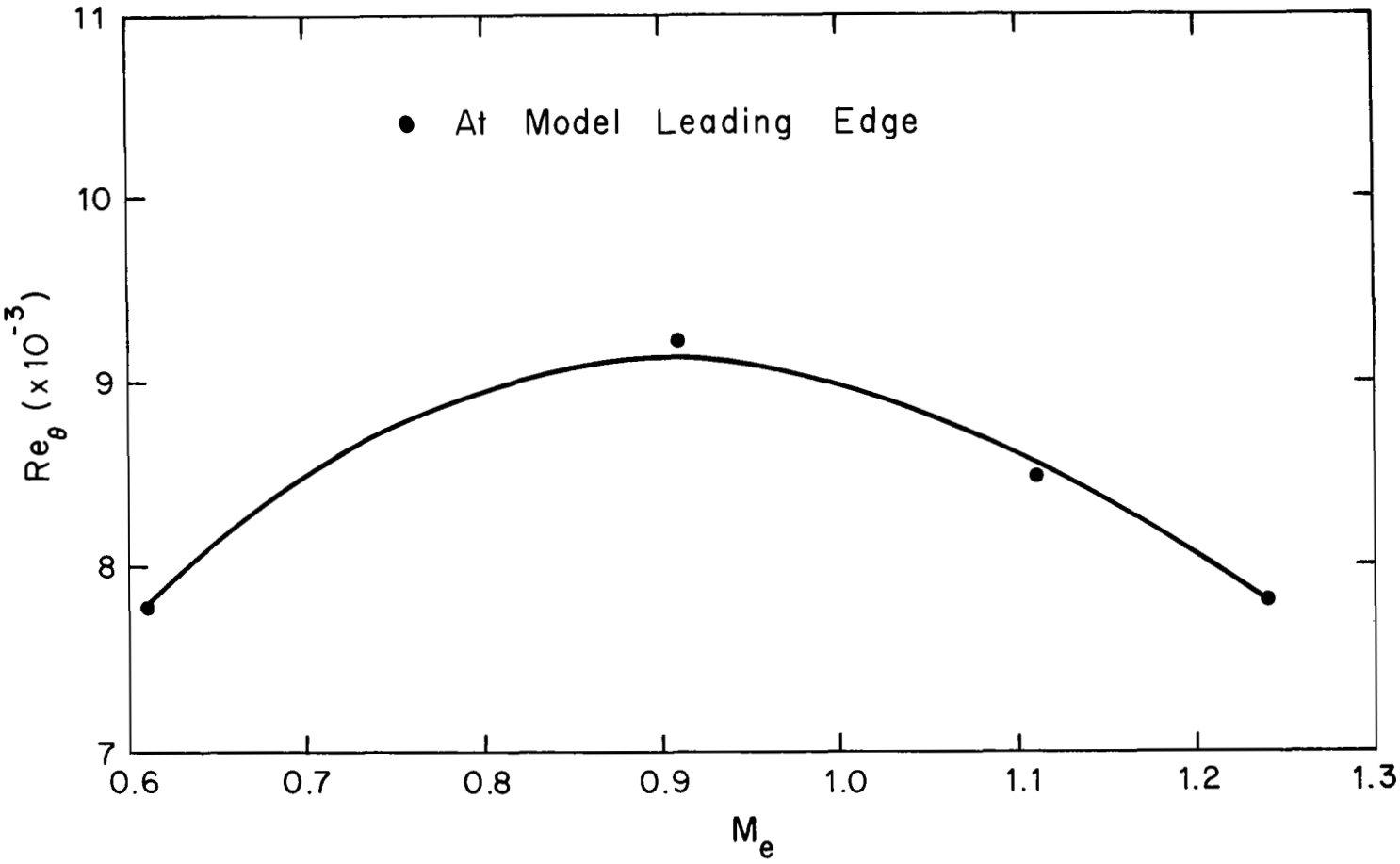

Figure 13. Transonic Momentum Thickness Reynolds Number

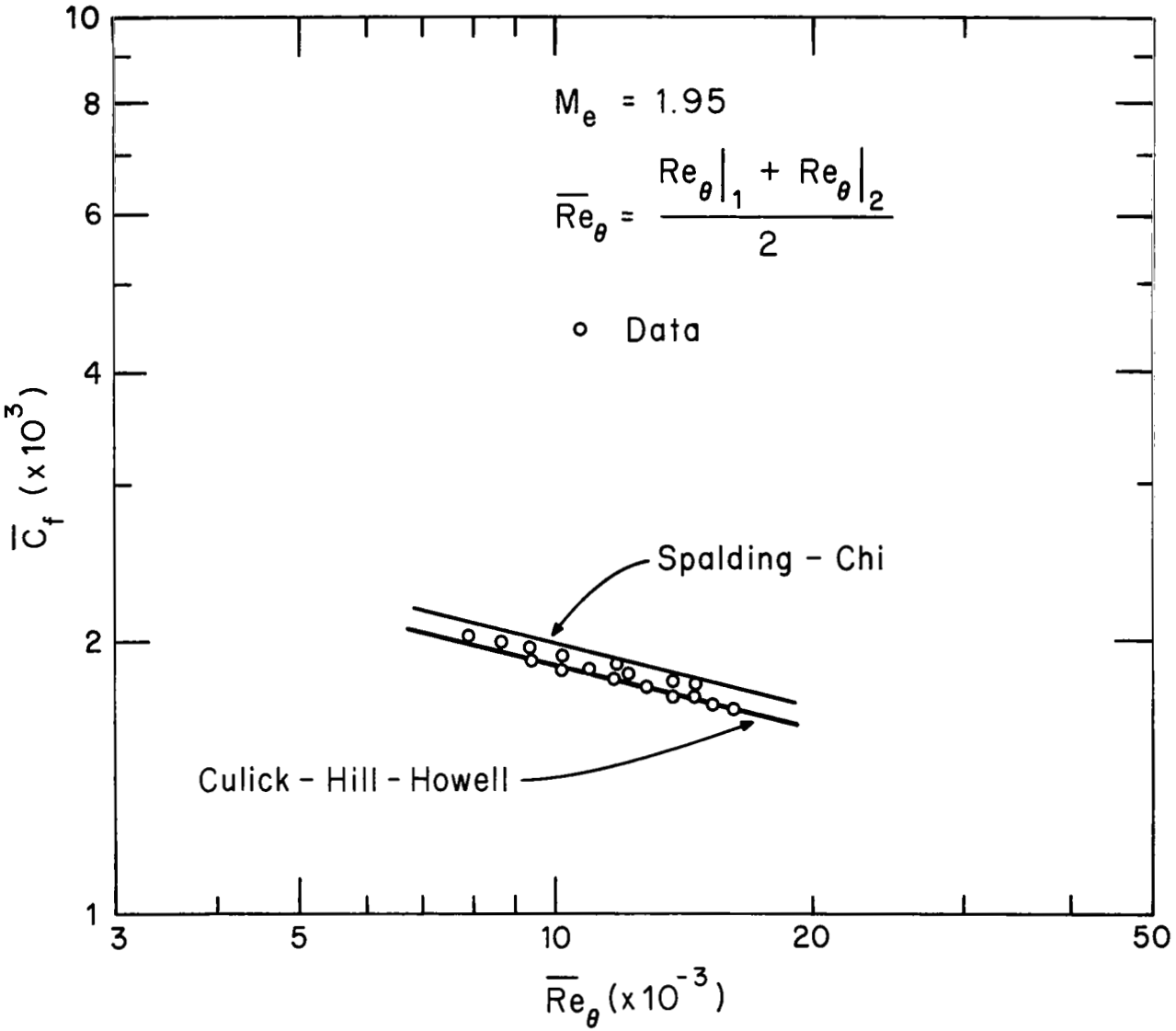

Figure 14. Average Drag Coefficient on a Flat Plate

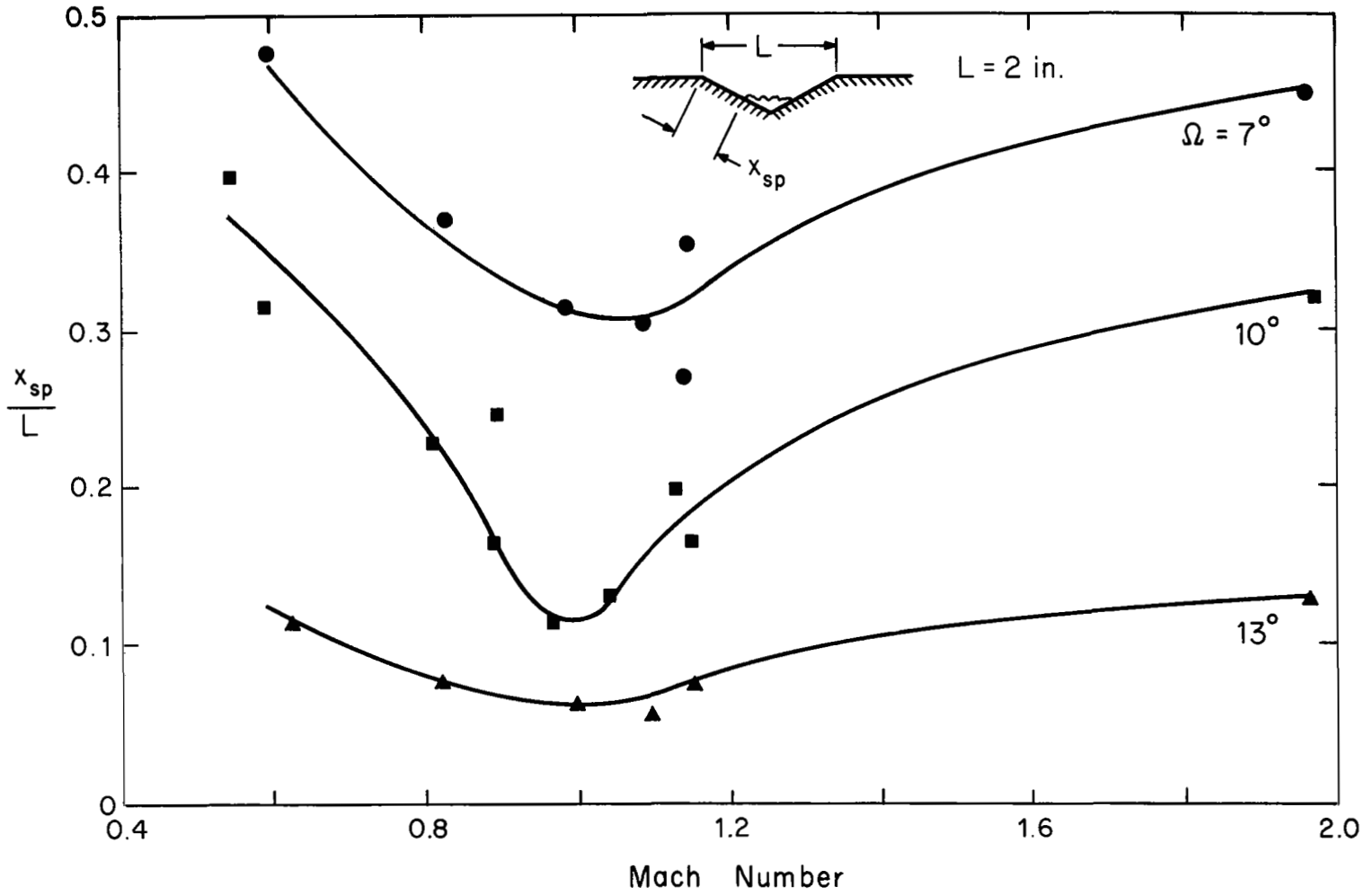

Figure 15. Self-adjustment of the Separation Point

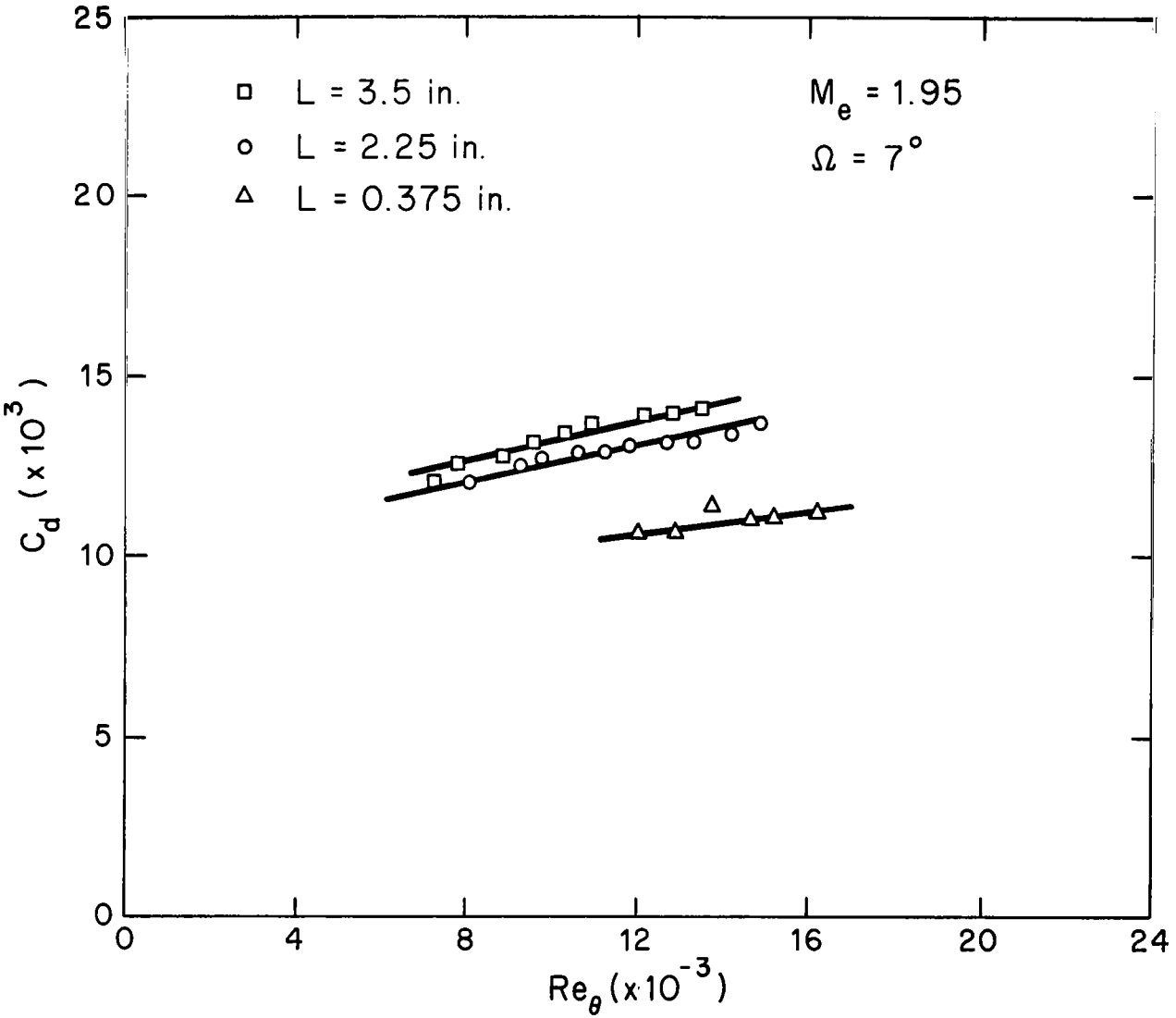

Figure 16. Supersonic Notch Drag Coefficients

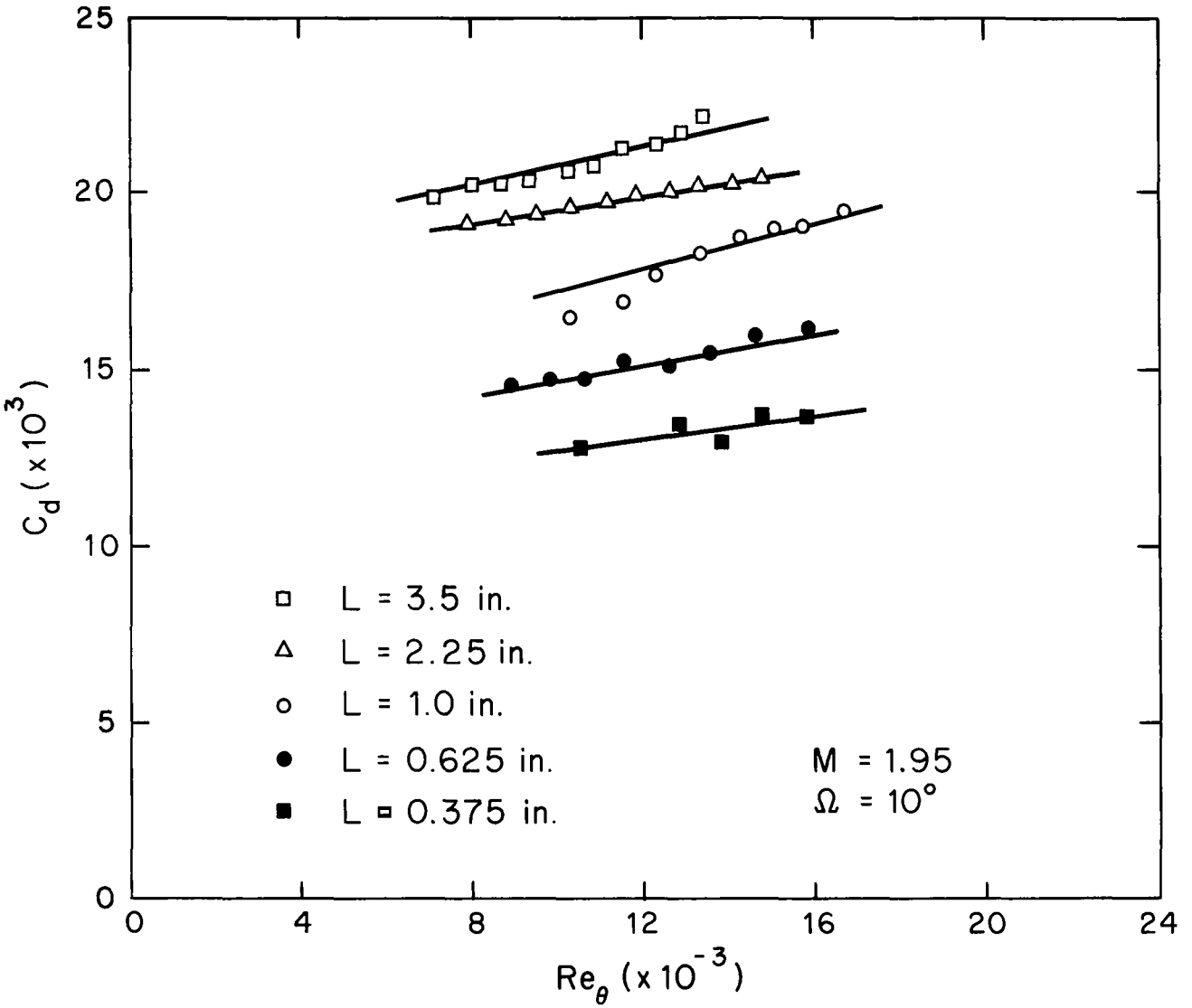

Figure 17. Supersonic Notch Drag Coefficients

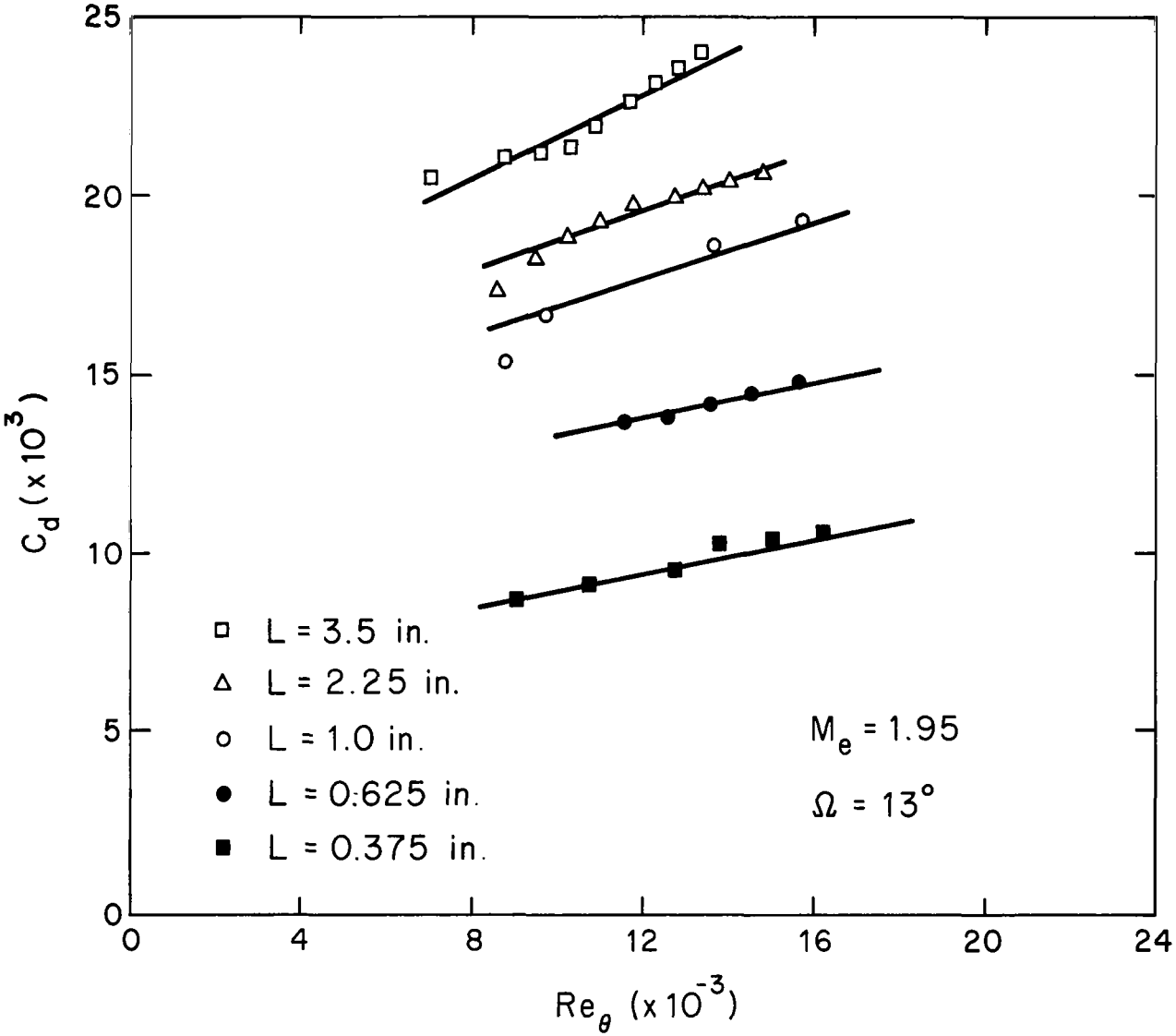

Figure 18. Supersonic Notch Drag Coefficients

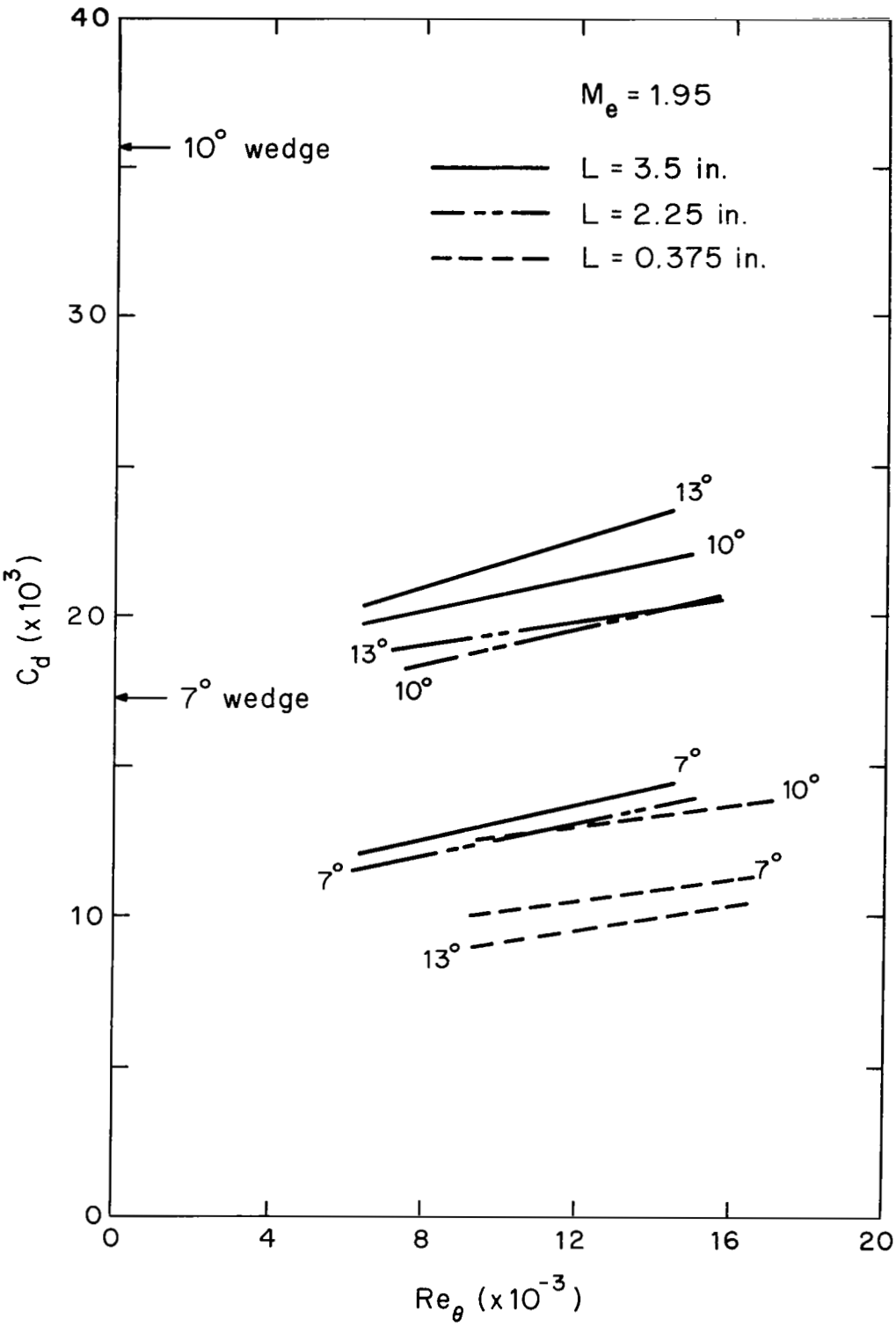

Figure 19. Summary of Supersonic C_d

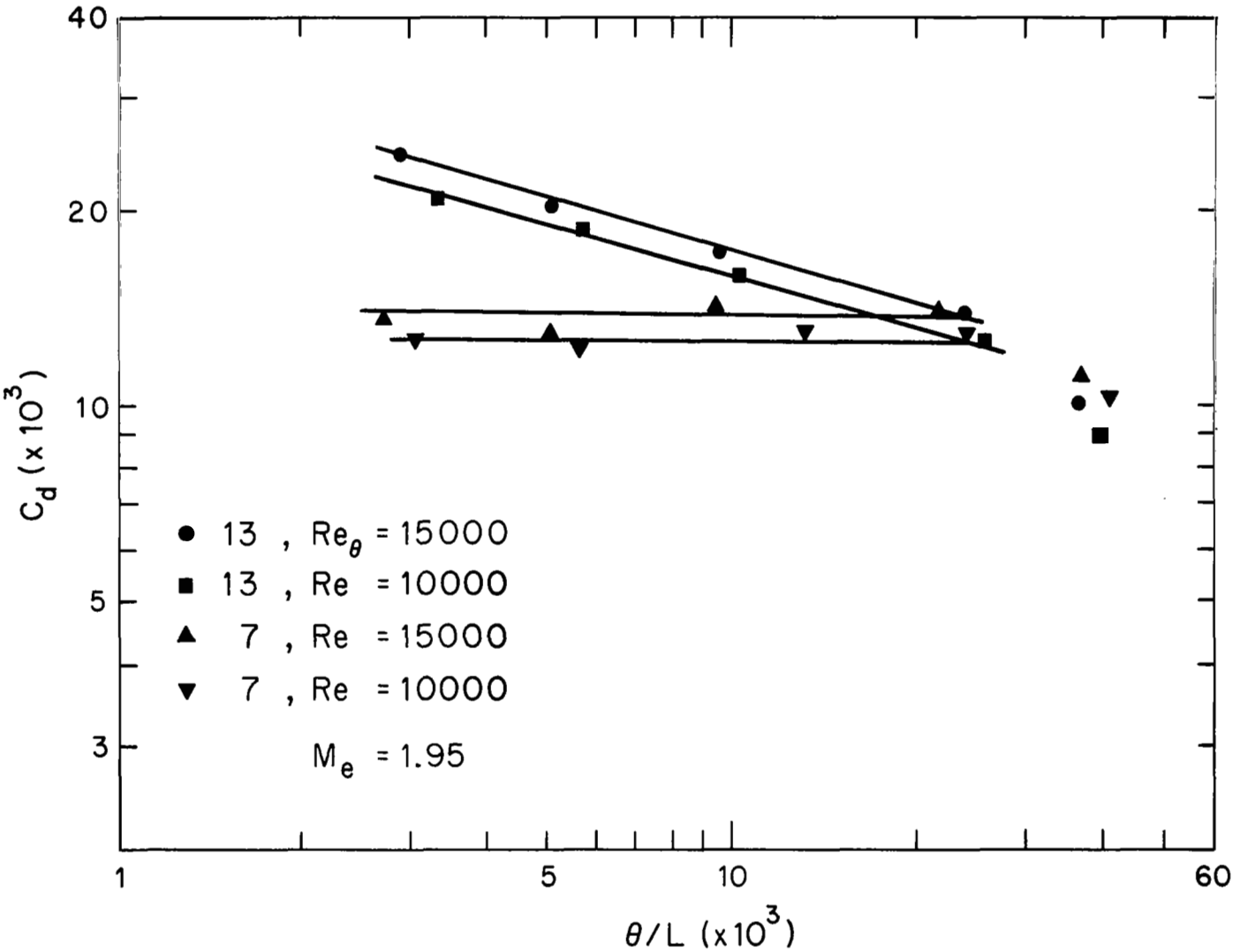

Figure 20. Shear Layer and Re_θ Effect on C_d

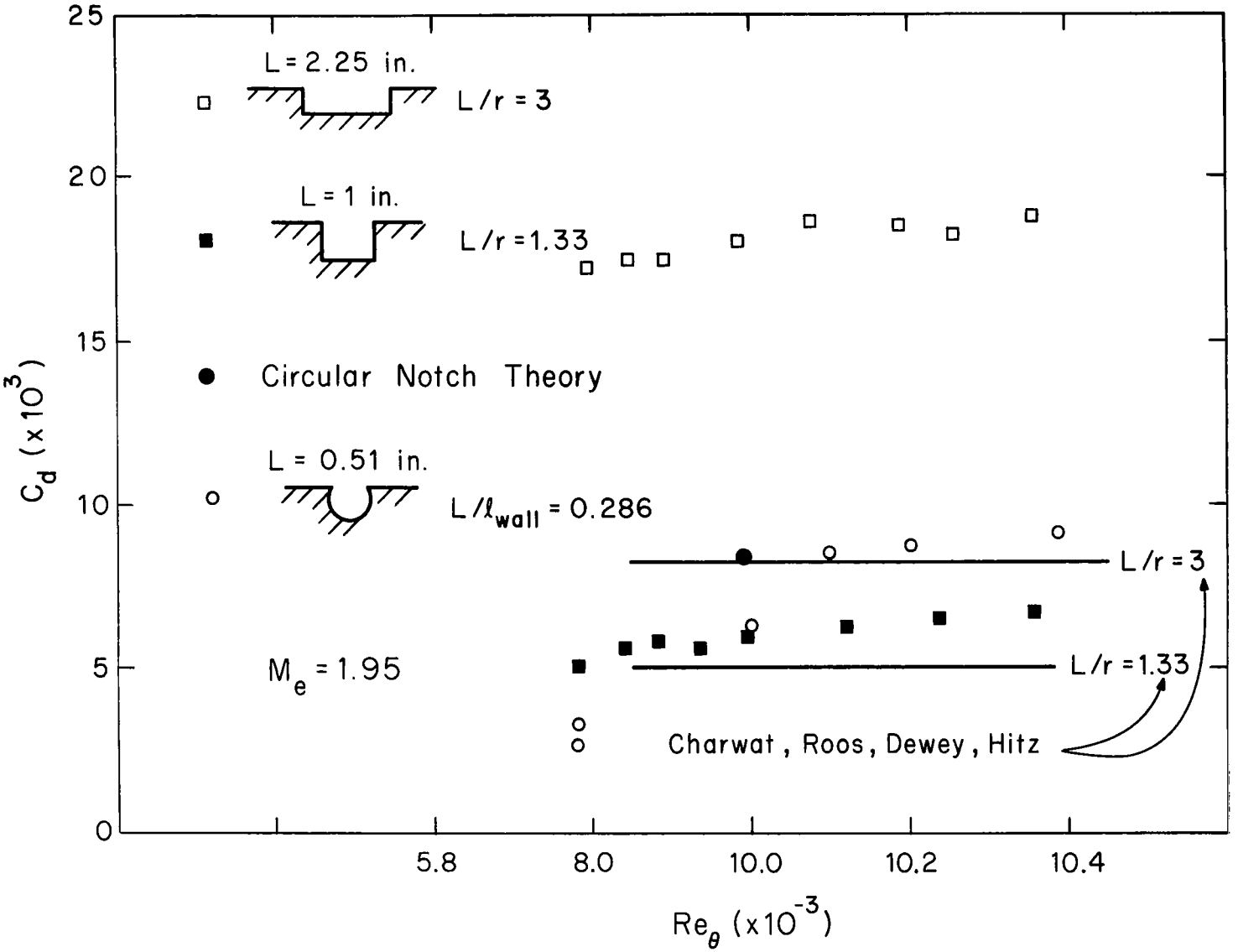

Figure 21. C_d for Rectangular and Circular Notches

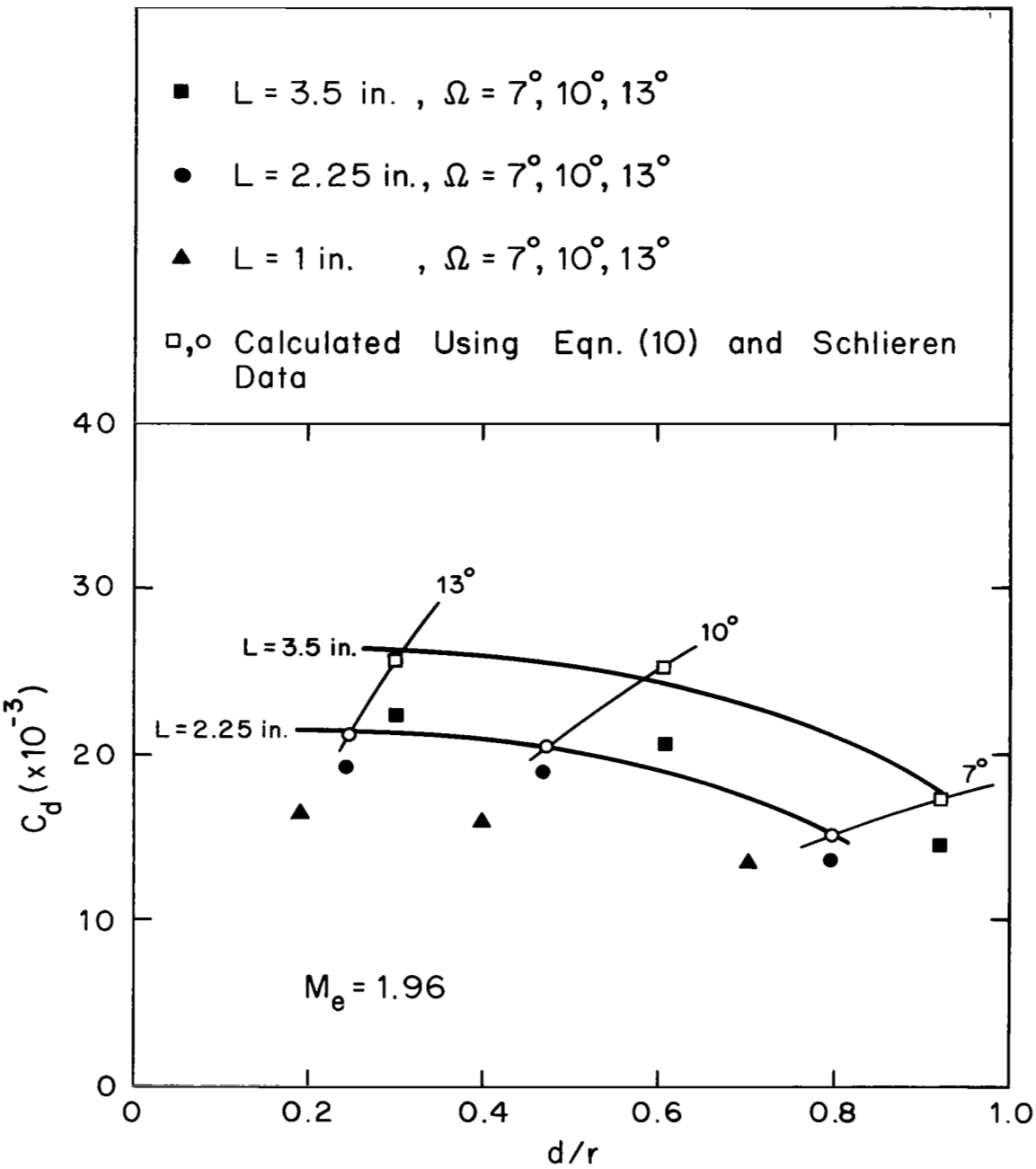

Figure 22. Theoretical and Experimental C_d

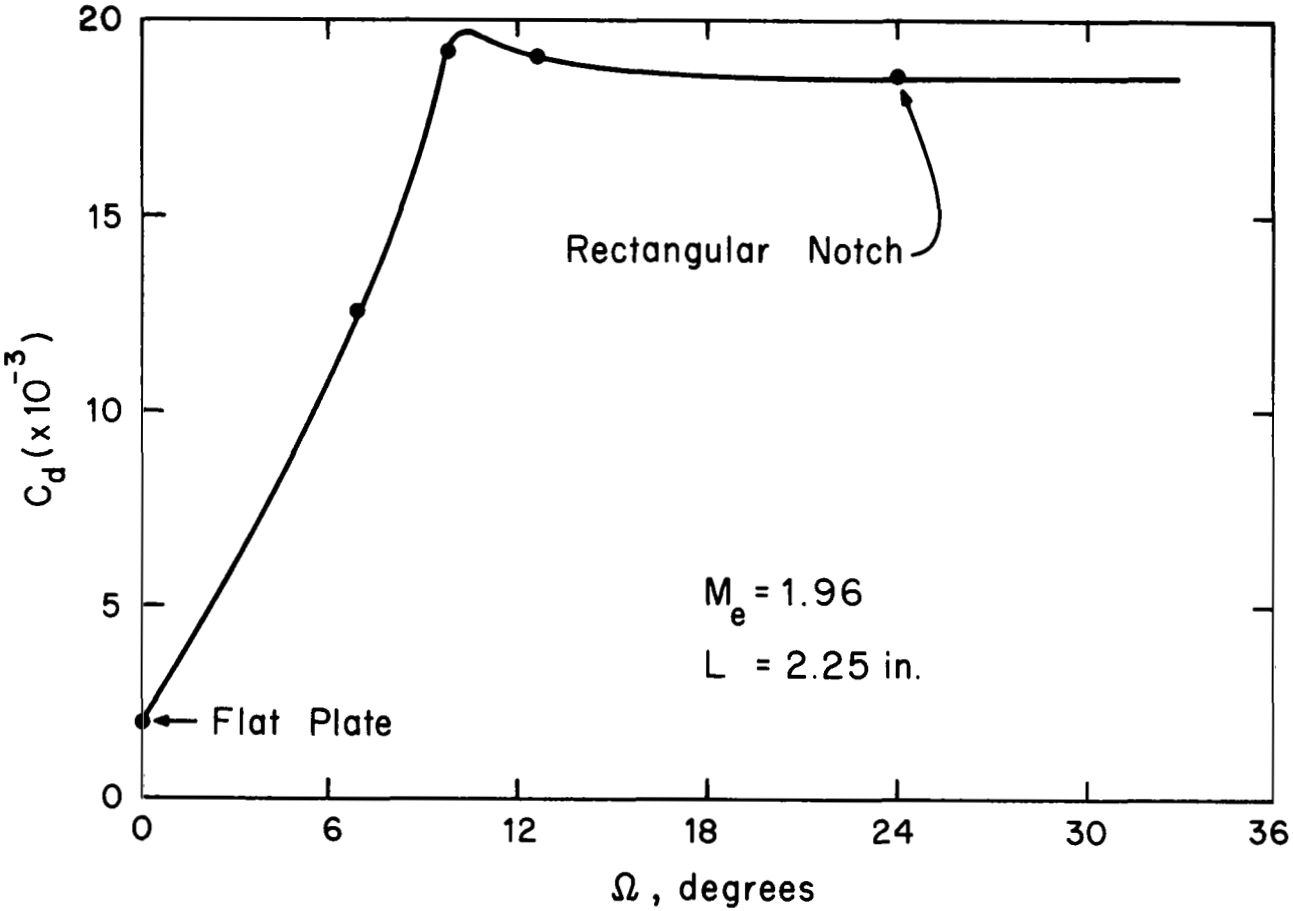

Figure 23. C_d Variation with Notch Angle

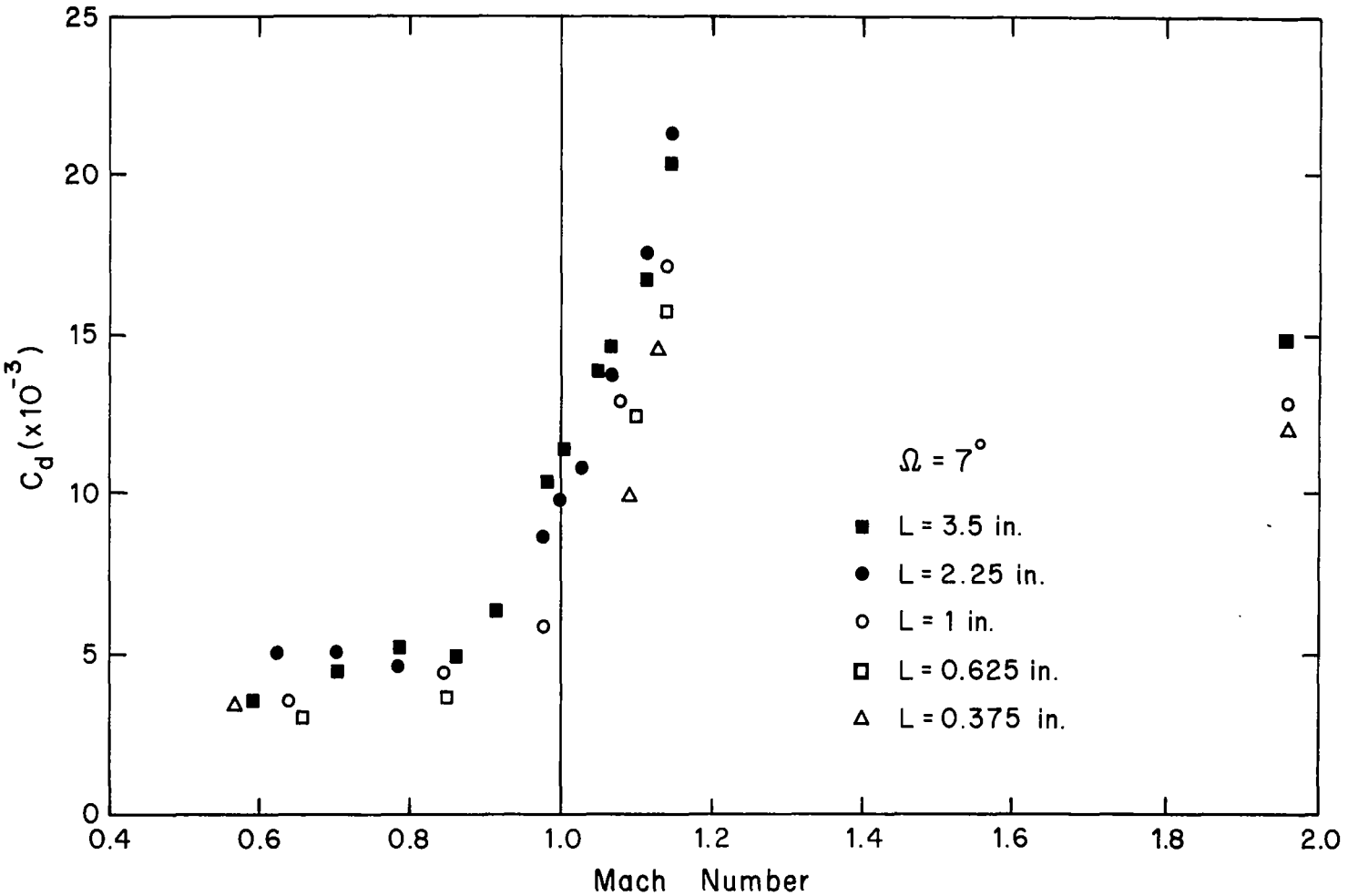

Figure 24. Transonic Notch Drag Coefficients

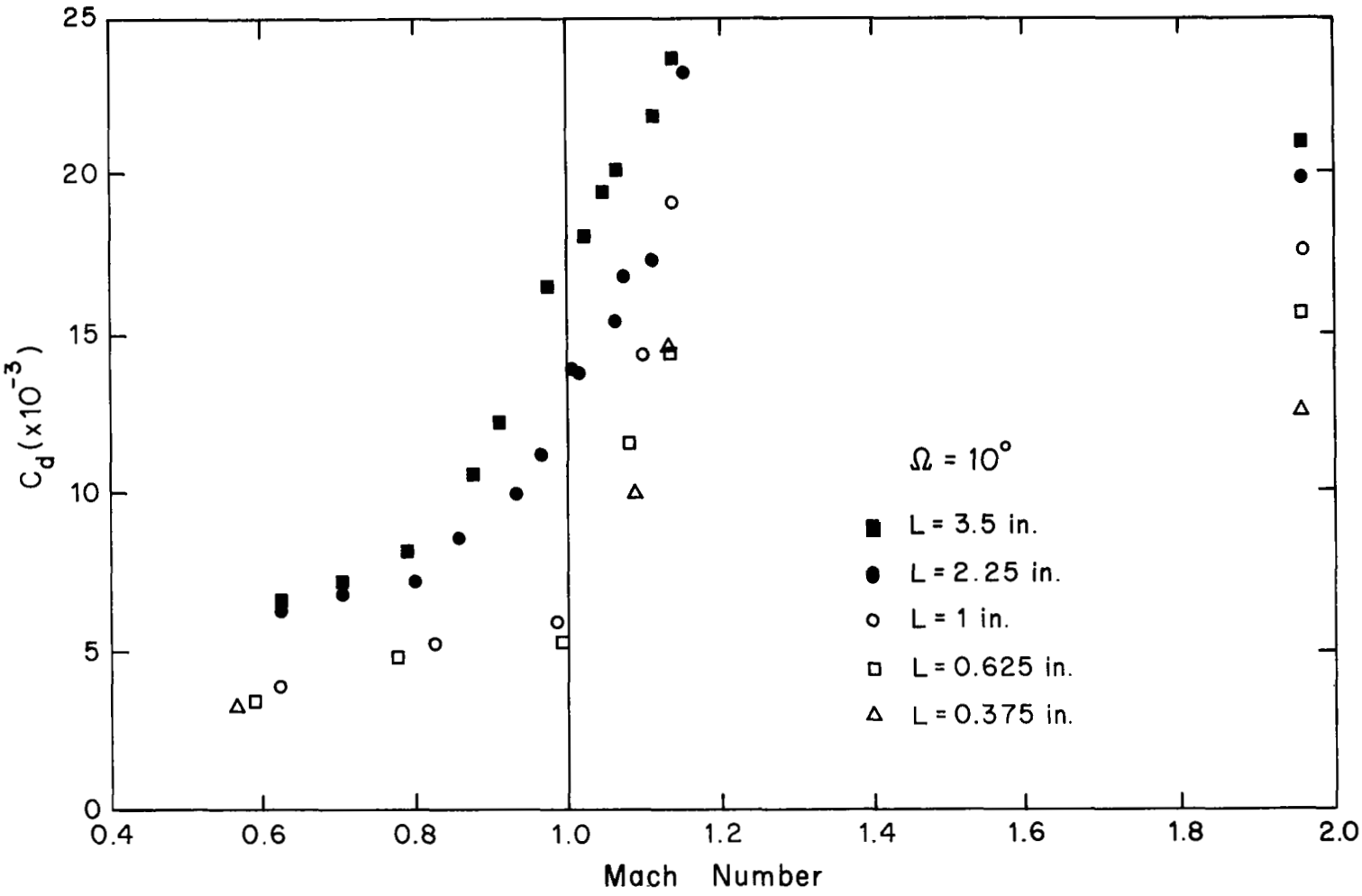

Figure 25. Transonic Notch Drag Coefficients

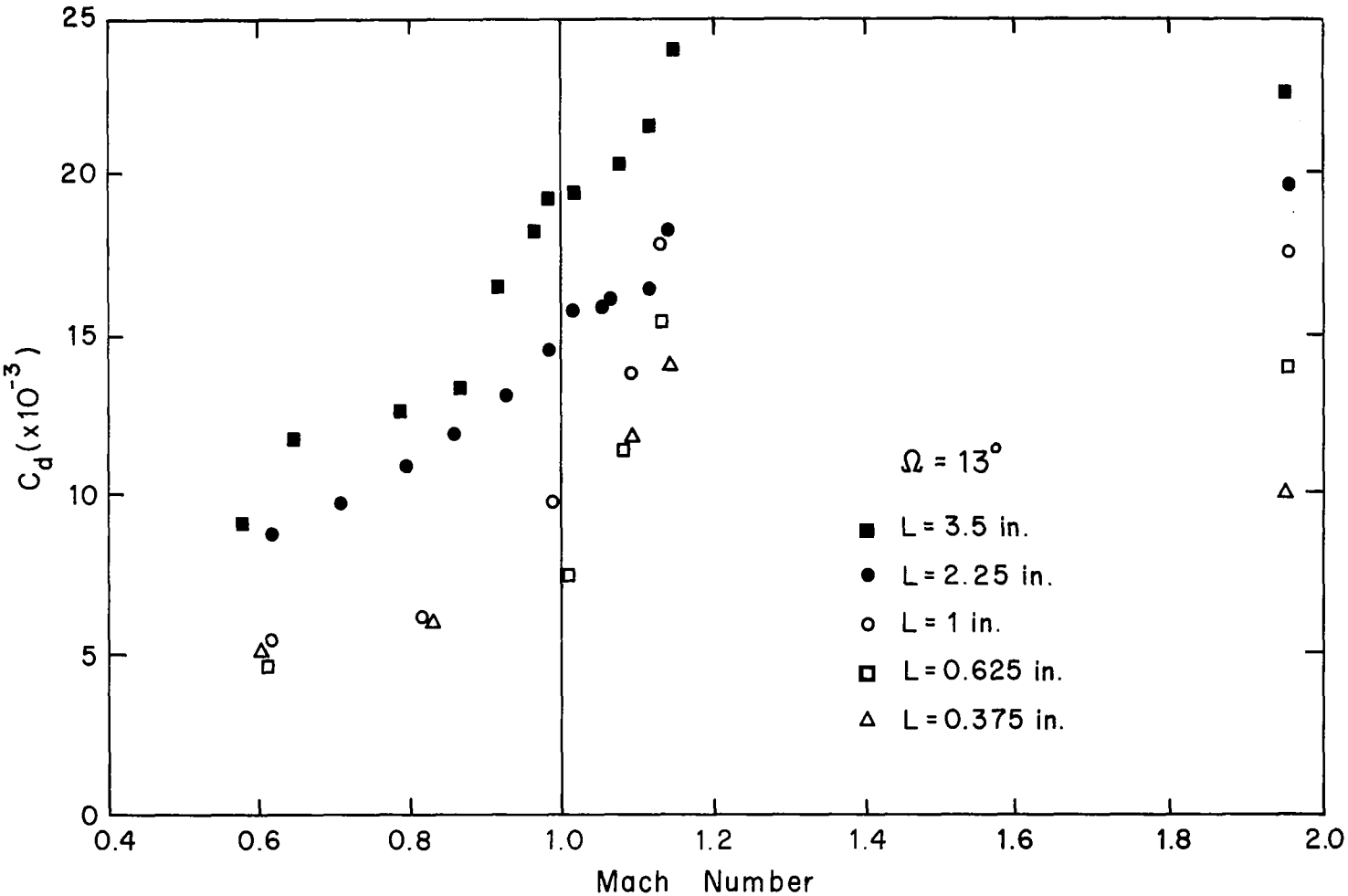

Figure 26. Transonic Notch Drag Coefficients

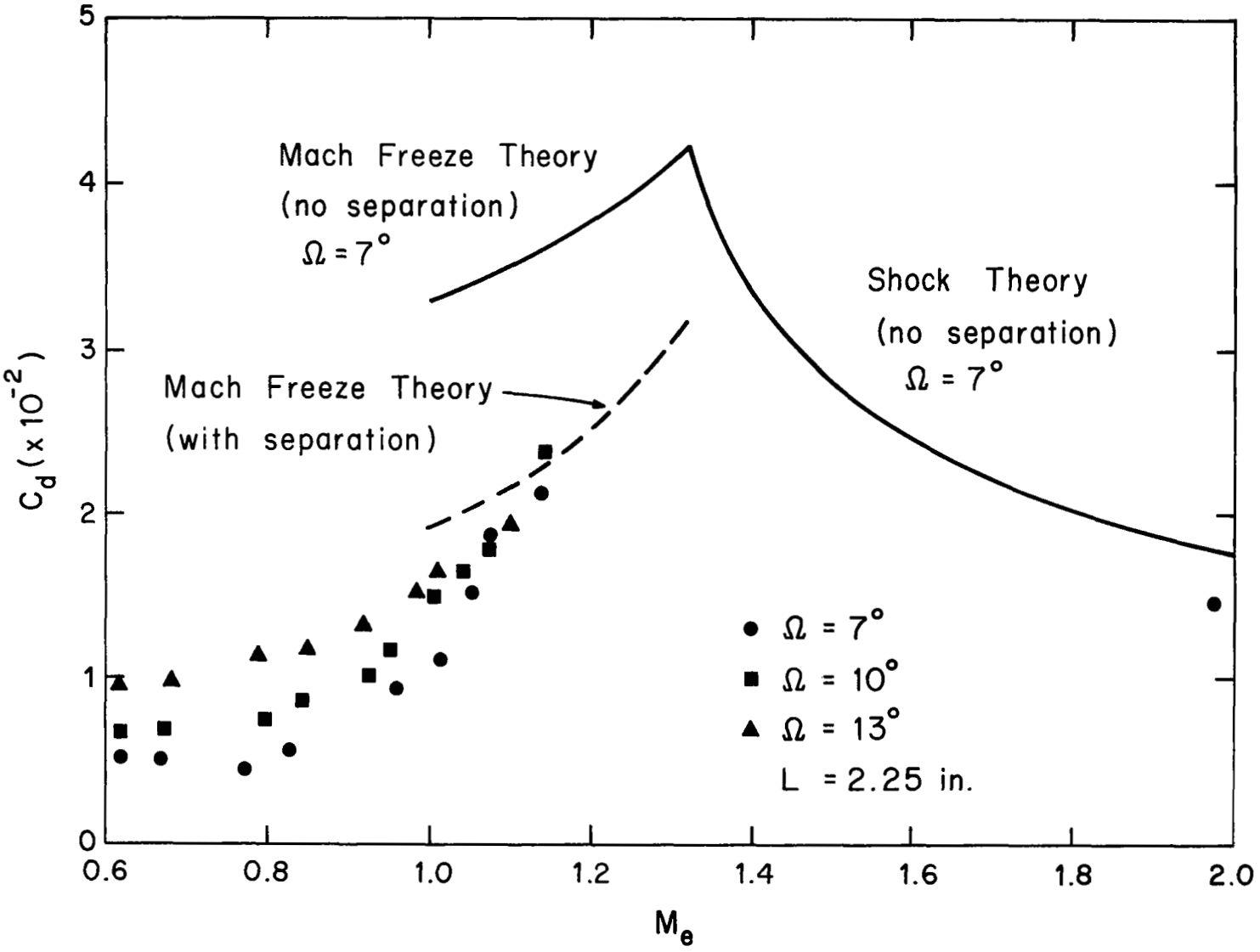

Figure 27. Comparison of C_d with Flow Model

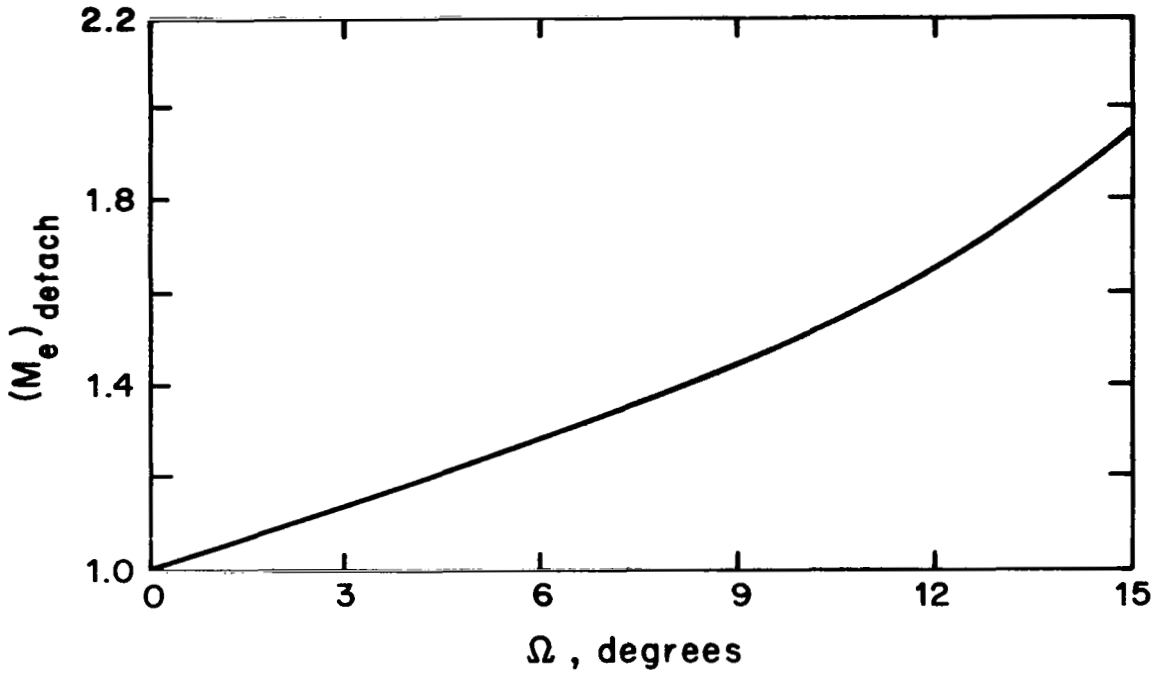

Figure 28. Detaching Mach Number

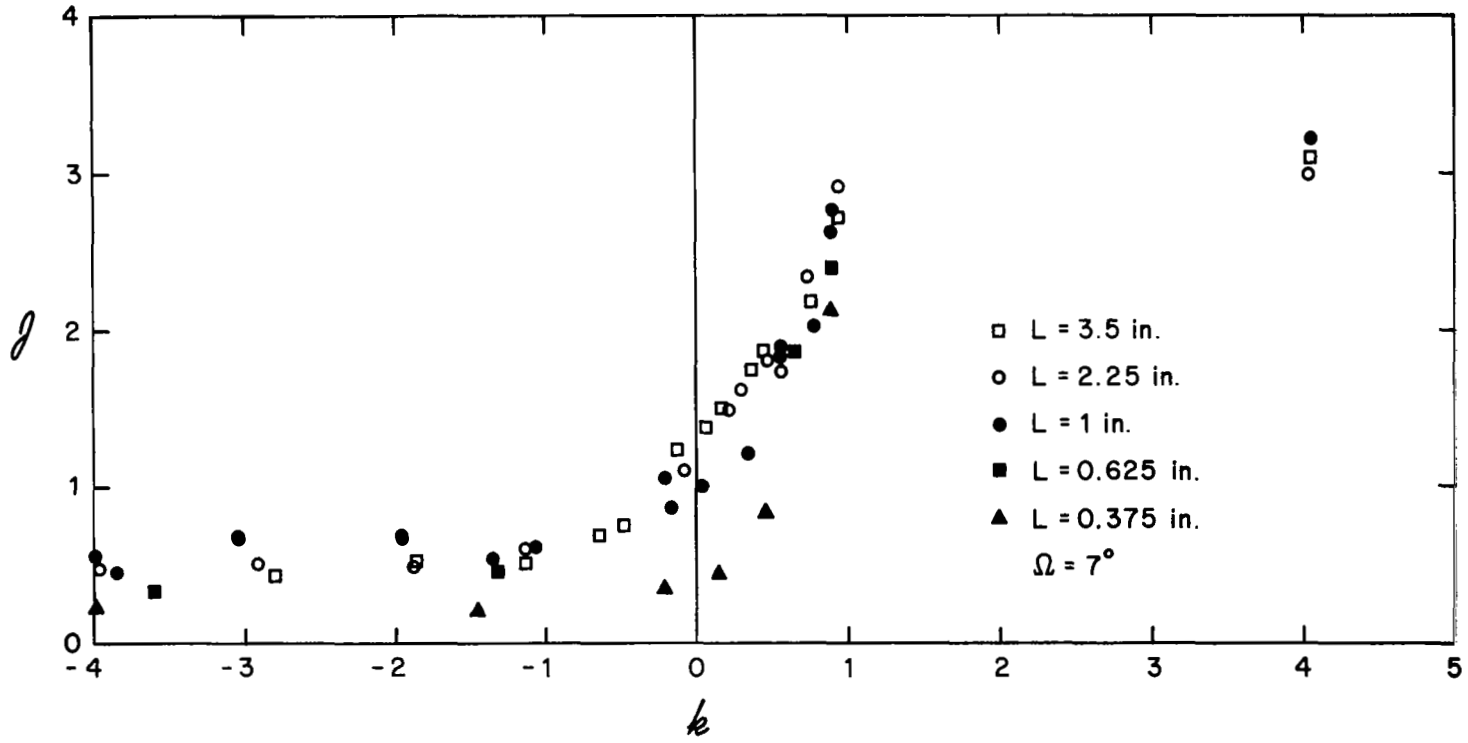

Figure 29. Transonic Similarity Parameters

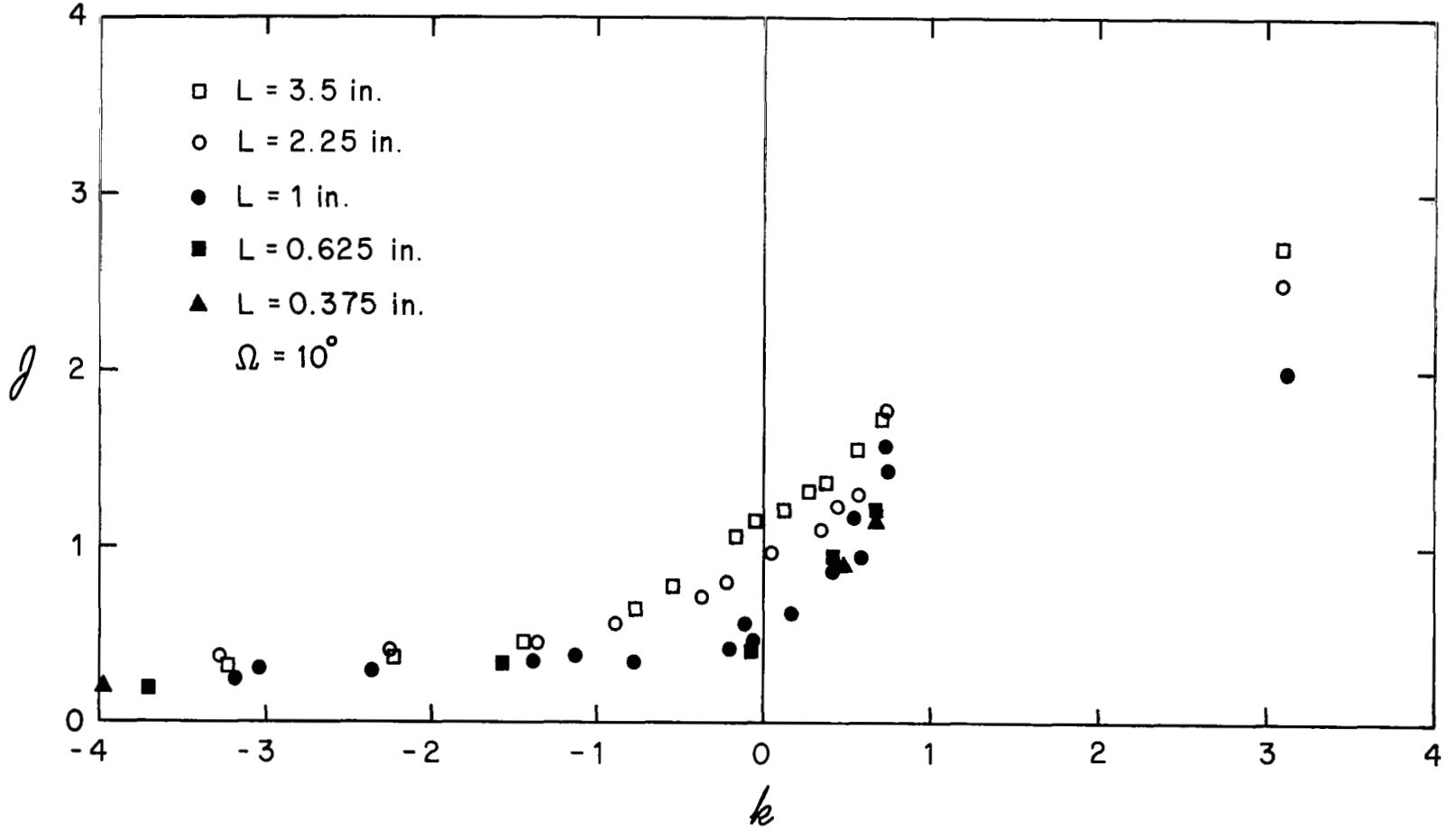

Figure 30. Transonic Similarity Parameters

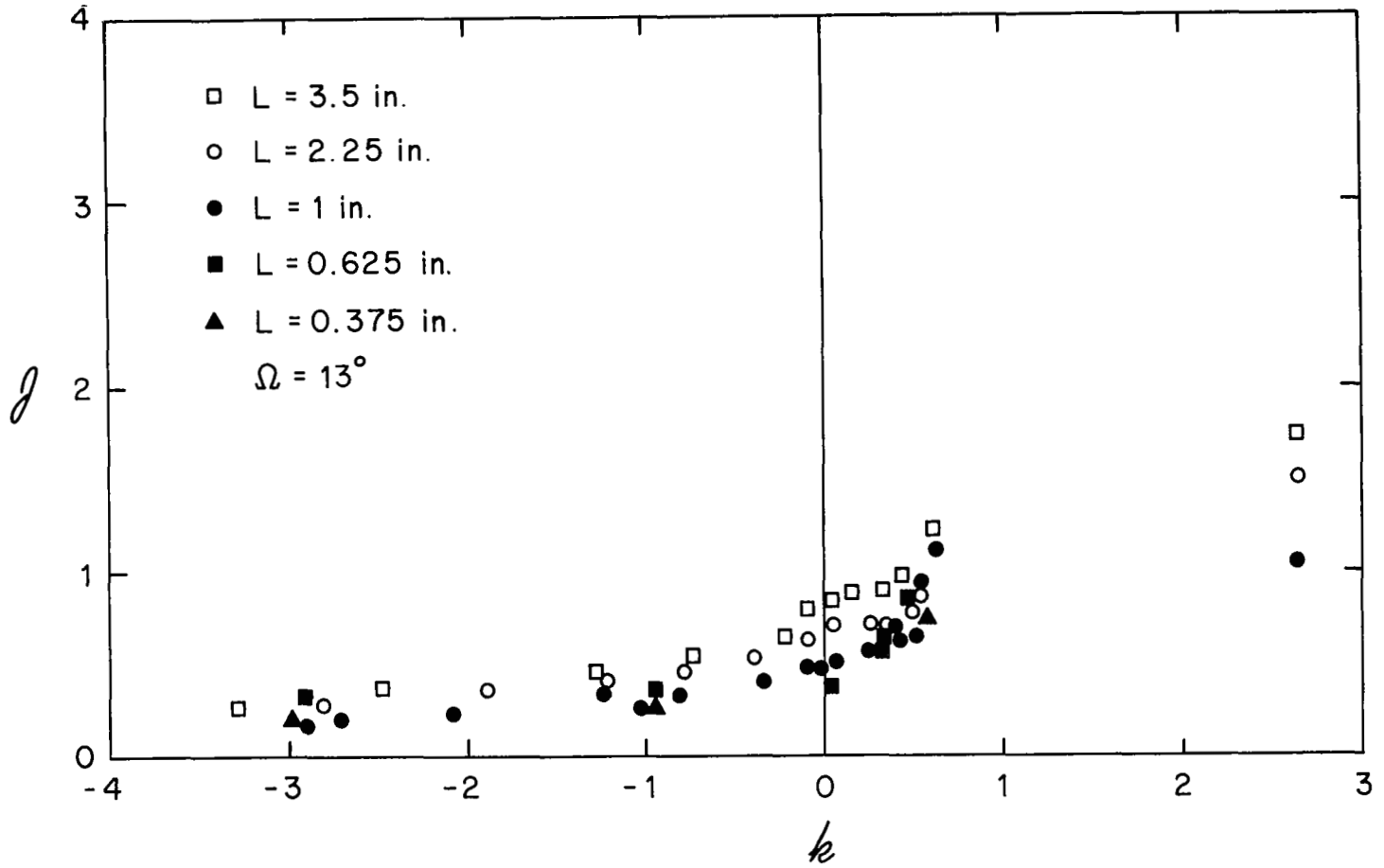

Figure 31. Transonic Similarity Parameters

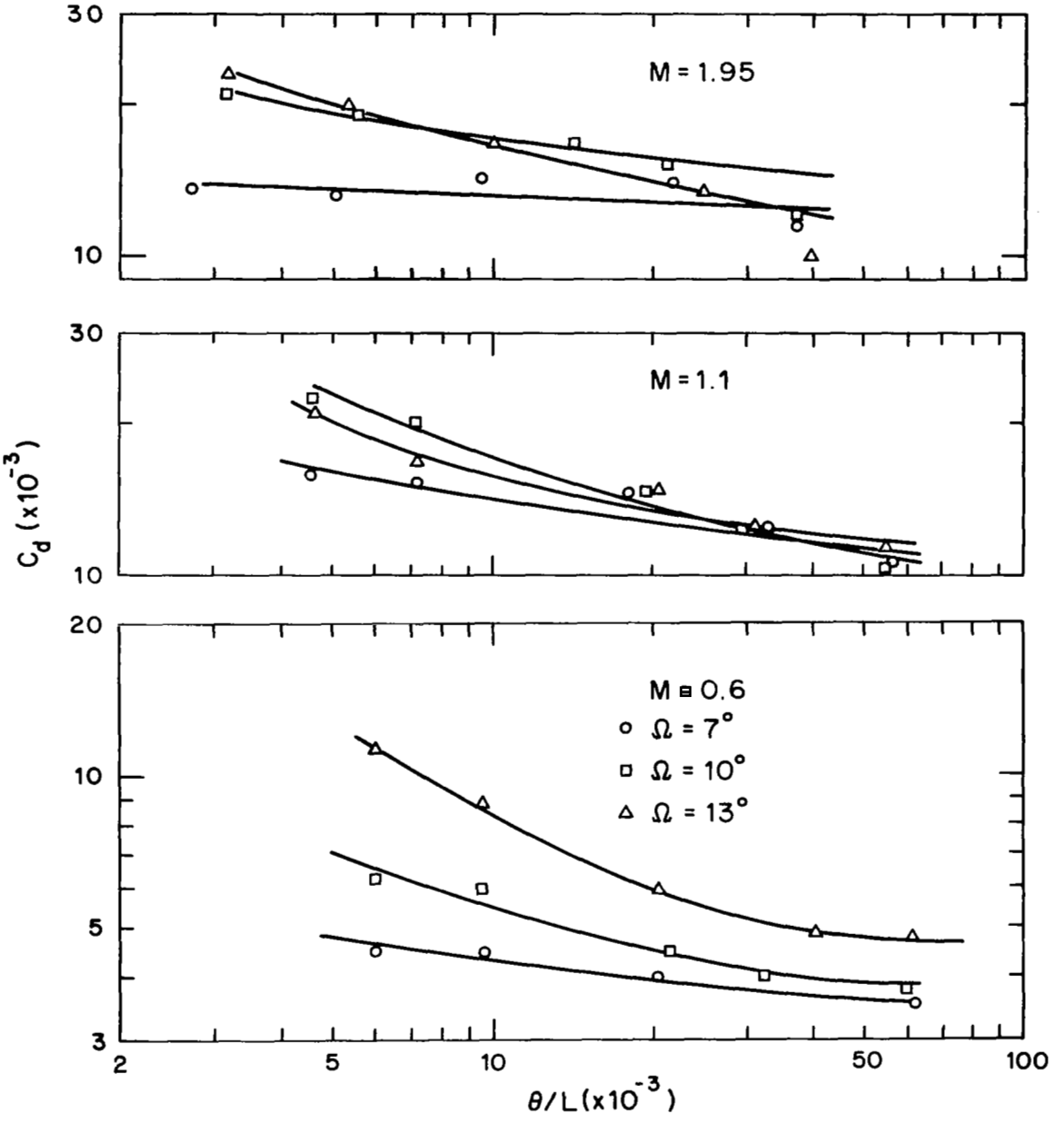

Figure 32. M_e and θ/L Effect on C_d

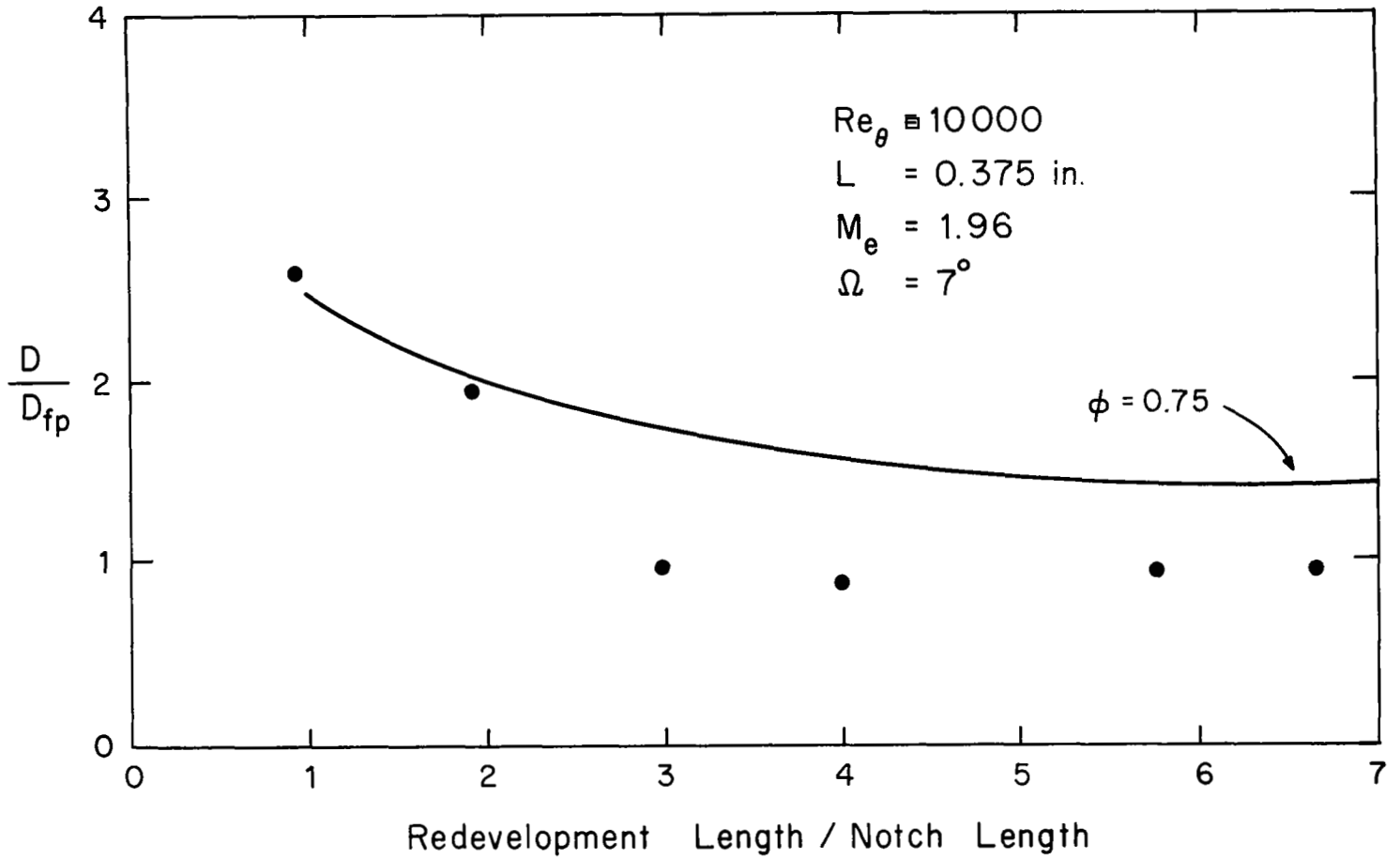

Figure 33. Redevelopment Drag Force
(D = drag force on redevelopment length, D_{fp} = drag force on flat surface equal to the redevelopment length at same tunnel location but without the notch upstream)